

Thermodynamic crossovers in supercritical fluids

Xinyang Li^{1,2} and Yuliang Jin^{1,2,3,*}

¹*CAS Key Laboratory of Theoretical Physics, Institute of Theoretical Physics,
Chinese Academy of Sciences, Beijing 100190, China*

²*School of Physical Sciences, University of Chinese Academy of Sciences, Beijing 100049, China*

³*Wenzhou Institute, University of Chinese Academy of Sciences, Wenzhou, Zhejiang 325000, China*

(Dated: April 30, 2024)

Can liquid-like and gas-like states be distinguished beyond the critical point, where the liquid-gas phase transition no longer exists and conventionally only a single supercritical fluid phase is defined? Recent experiments and simulations report strong evidence of dynamical crossovers above the critical temperature and pressure [1–3]. Despite using different criteria, many existing theoretical explanations consider a single crossover line separating liquid-like and gas-like states in the supercritical fluid phase [4–10]. We argue that such a single-line scenario is inconsistent with the supercritical behavior of the Ising model, which has two crossover lines due to its symmetry, violating the universality principle of critical phenomena. To reconcile the inconsistency, we define two thermodynamic crossover lines in supercritical fluids as boundaries of liquid-like, indistinguishable and gas-like states. Near the critical point, the two crossover lines follow critical scalings with exponents of the Ising universality class, supported by calculations of theoretical models and analyses of experimental data from the standard database [11]. The upper line agrees with crossovers independently estimated from the inelastic X-ray scattering data of supercritical argon [1, 2], and from the small-angle neutron scattering data of supercritical carbon dioxide [3]. The lower line is verified by the equation of states for the compressibility factor. This work provides a fundamental framework for understanding supercritical physics in general phase transitions.

According to textbook knowledge, no liquid-gas phase transitions exist in the supercritical fluid state of matter. Then, how does a liquid transform into a gas (or vice versa) along a path by passing the critical point? Many studies propose that there should be a line of *supercritical crossovers* between liquid-like and gas-like states. Such a crossover line divides the phase diagram above the critical point into regimes with different physical properties, which can be connected without going through any thermodynamic singularity. The following supercritical crossover lines have been defined.

(I) *Widom line* [4, 12–21] (see Fig. 1A), defined as the line of maxima in isobaric specific heat C_P under the fixed pressure P (or temperature T) condition. The maximum value increases approaching the critical point, and diverges at the point. The lines of maxima determined according to different response functions are assumed to converge into a single line near the critical point, which emanates from the critical point.

(II) *Fisher-Widom line* [5, 22–27], defined as the boundary between states with exponential (gas-like) and oscillatory (liquid-like) long-range decays of the pair correlation function. Liquid-like and gas-like states are distinguished based on the structure of configuration, i.e., the spatial distribution of particles.

(III) *Frenkel line* [6, 28–38], which separates liquid-like and gas-like states based on whether viscoelastic dynamics are present. Within the vibrational time, liquids behave like amorphous solids – particles vibrate around their equilibrium positions; beyond the structural relax-

ation time (diffusion time), particles diffuse, and the equilibrium configuration decorrelates from the initial one. As T increases (or P decreases), this liquid-like picture breaks down at the Frenkel line, where the vibration time becomes comparable with the structural relaxation time, and the system turns into a gas-like state.

(IV) *Nishikawa line* [7, 39, 40], defined by the “ridge” of the density fluctuation profile on the P - T phase diagram, where the density fluctuation maximizes.

(V) *Symmetry line* [8], defined at the zero skewness in the particle number distribution for the grand canonical ensemble. Liquid-like behavior is characterized by a negative skewness indicating the favor of particle deletion, whereas gas-like behavior is characterized by a positive skewness indicating the favor of particle insertion.

(VI) *Percolation lines* [9, 41], determined by the loci of the percolation transition of available volume accessible to any single mobile atom, and that of the cluster formed by bonded atoms. The percolation line of the hydrogen bond network has also been studied in supercritical water [10], but the method cannot be applied to supercritical fluids without hydrogen bonds.

(VII) Boundaries of the pseudo-boiling transitional region [15, 42]. The transition upon crossing the Widom line has been referred to as supercritical pseudo-boiling [15], a phenomenon obeying similar laws as subcritical boiling, according to which the Widom line is also named as a *pseudo-boiling line*. At a constant pressure P , the pseudo-boiling transition starts at a temperature $T^-(P)$, where the isobaric specific heat C_P starts to deviate from its liquid value, and ends at $T^+(P)$, when C_P approaches its ideal gas value. The two lines, $T^\pm(P)$, are *pseudo-boiling boundaries*.

* yuliangjin@mail.itp.ac.cn

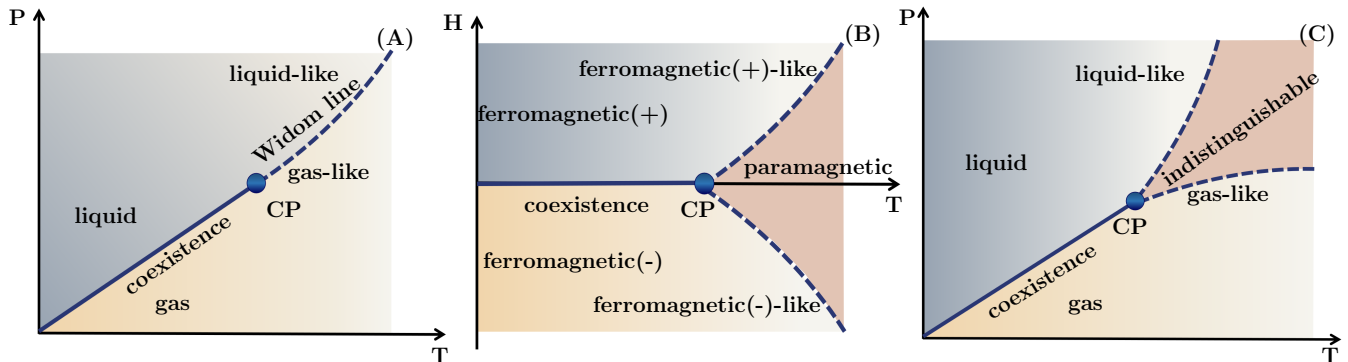


FIG. 1. **Schematic phase diagrams.** (A) Liquid-gas (pressure P vs temperature T) phase diagram with a Widom line (dashed) separating liquid-like and gas-like regimes above the critical point (CP). (B) Phase diagram of the Ising model, with two supercritical crossover lines (dashed) separating positive ferromagnetic-like, paramagnetic, and negative ferromagnetic-like regimes. (C) Liquid-gas phase diagram with two supercritical crossover lines (dashed), L^\pm , separating liquid-like, indistinguishable, and gas-like regimes.

The liquid-gas system and the Ising model both exhibit a critical point. The liquid-gas transition is not associated with the change of structural order, while the magnetic phase transition in the Ising model is of the order-disorder type. Despite this difference, the liquid-gas critical point and the magnetic phase transition in the three-dimensional (3D) Ising model belong to the same $O(1)$ universality class [43, 44]. According to the principle of universality in statistical mechanics, they should display critical scalings with the same exponents. In Ref. [17], a general linear scaling theory and molecular dynamics simulations are employed to obtain the Widom line for different kinds of critical points, including the liquid-gas critical point where the slope of the coexistence line is positive in the P - T plane (see Fig. 1A for the supercritical branch of the Widom line), the liquid-liquid critical point where the slope is negative, and the magnetic phase transition in the Ising model where the slope is zero (see Fig. 1B) [17]. However, the behavior of the Widom line is non-universal in the three cases. In general, the above proposals (I-VII) of crossover lines in supercritical fluids are all theoretically inconsistent with the supercritical crossover lines of the Ising model. To show that, let us first discuss the analogies between the two systems, and the supercritical behavior of the Ising model.

The pressure P and susceptibility $\kappa_T \equiv \frac{P_c}{\rho_c} \left(\frac{\partial \rho}{\partial P} \right)_T$ (or the compressibility $\beta_T = \frac{1}{\rho} \left(\frac{\partial \rho}{\partial P} \right)_T$) in liquid-gas systems are analogous of the magnetic field H and magnetic susceptibility $\chi = \left(\frac{\partial m}{\partial H} \right)_T$ in the Ising model, where P_c and ρ_c are the critical pressure and density. Here P and H play the role of external fields; κ_T and χ characterize the response of the order parameter (i.e., the liquid-gas density difference $\delta\rho$ and the magnetization m respectively) to the external field. Following the definition of Widom line, it is immediately apparent that in the Ising model, the maxima of χ at constant H form two crossover lines (denoted by L^+ and L^-) above the critical temperature

T_c . Due to the Z_2 symmetry of the Ising model, the two lines L^\pm are perfectly symmetric with respect to the coexistence line $H = 0$. Along L^\pm lines, the field and order parameter follow critical scalings,

$$|H^\pm| \sim (T - T_c)^{\beta+\gamma}, \quad (1)$$

and

$$|m^\pm| \sim (T - T_c)^\beta, \quad (2)$$

established by analytic calculations of the mean-field model and Monte-Carlo numerical simulations of 2D and 3D models (see Supplementary Information SI Sec. S1), where β and γ are universal critical exponents (for the 3D Ising universality class, $\beta \simeq 0.3265$ and $\gamma \simeq 1.237$ [45]).

The L^\pm lines in the Ising model have the following properties. (i) They separate three states, positive ferromagnetic-like, paramagnetic and negative ferromagnetic-like states (see Fig. 1B). (ii) The two lines coincide only at the critical point. They do not merge to a common line even in the vicinity of the critical point. (iii) The two lines follow the critical scalings Eqs. (1) and (2). None of the above-mentioned supercritical crossover lines (I-VII) simultaneously satisfy all these three properties (see SI Table S1 for a summary). Definitions (I-V) give one single crossover line; definition (VI) gives two percolation lines, but they do not emanate from the critical point. The (II) Fisher-Widom line, (III) Frenkel line, and (VI) percolation lines do not pass through the critical point, and thus are without any critical scaling. The (I) Widom line, (IV) Nishikawa line, (V) symmetry line, and (VII) pseudo-boiling boundaries $T^\pm(P)$, although emanating from the critical point, do not satisfy the critical scalings Eqs. (1) and (2). In short, even though it is well established that liquid-gas and ferromagnetic-paramagnetic critical points belong to the same 3D Ising universality class, their supercritical physics is not yet unified within the framework of critical universality.

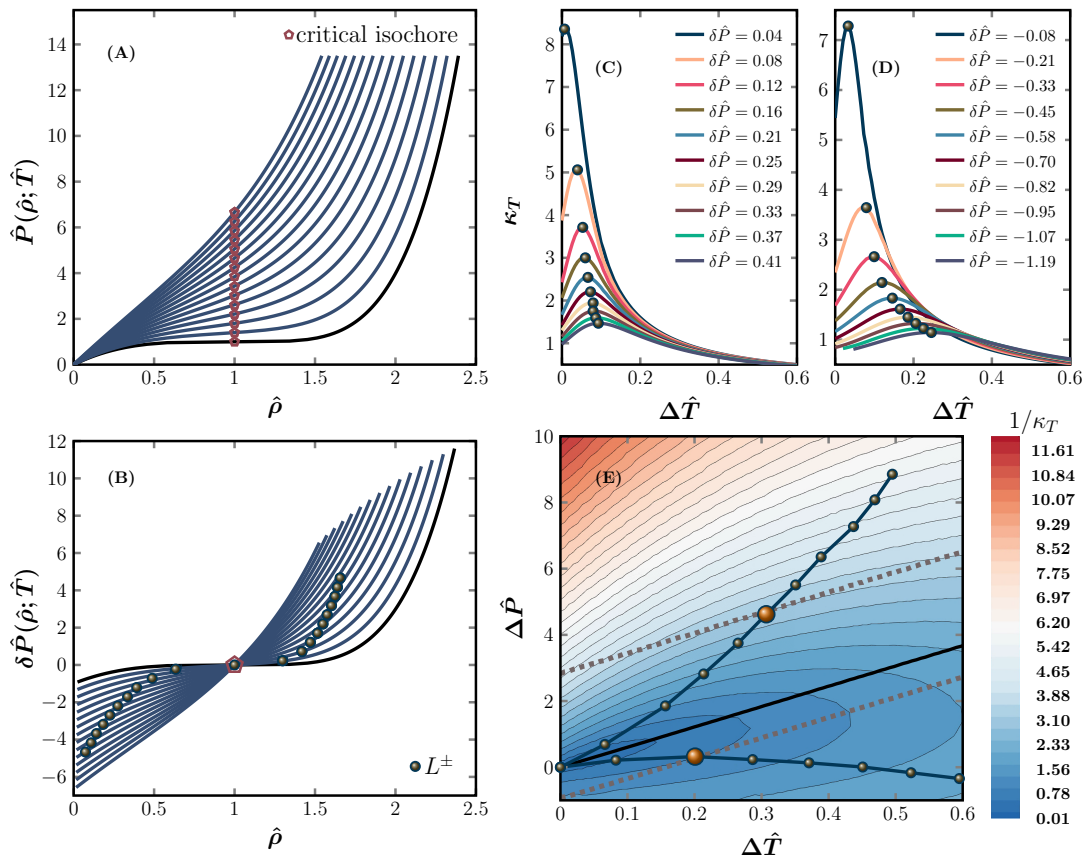


FIG. 2. **Determination of supercritical crossover lines L^\pm in argon.** (A) Isothermal EOSs, $\hat{P}(\hat{\rho}; \hat{T})$, for $\hat{T} = 1.00, 1.07, 1.13, 1.20, 1.27, 1.33, 1.40, 1.46, 1.53, 1.60, 1.66, 1.73, 1.80, 1.86, 1.93$. (from bottom to top). (B) Shifted EOSs $\delta\hat{P}(\hat{\rho}; \hat{T})$. (C-D) Susceptibility κ_T as a function of $\Delta\hat{T}$, for a few fixed $\delta\hat{P}$. The loci of peaks determine (C) L^+ and (D) L^- lines, for $\delta\hat{P} > 0$ and $\delta\hat{P} < 0$ respectively. (E) The color map of $1/\kappa_T$ in the $\Delta\hat{P} - \Delta\hat{T}$ diagram, with constant $1/\kappa_T$ contour lines (solid thin lines). As an example, we show two parallel paths (dashed brown lines) to the critical isochore (think black line). Such a parallel path has a point of tangency (big orange ball) with a certain constant $1/\kappa_T$ contour; along this parallel path, the point of tangency corresponds to the maximum of κ_T as defined in L^\pm . In panels (B-E), the L^\pm lines are represented by the same symbol.

METHODS AND RESULTS

To resolve the inconsistency, we propose a new definition of the crossover lines in supercritical fluids (see Fig. 1C). The method is explained in Fig. 2, taking argon as an example. The general procedure is as follows. (i) The experimental data of supercritical isothermal equations of states (EOSs), $\hat{P}(\hat{\rho}; \hat{T})$, are collected from the National Institute of Standards and Technology (NIST) database [11] and plotted in Fig. 2(A), where the state variables are rescaled by their critical values, $\hat{T} = T/T_c$, $\hat{P} = P/P_c$ and $\hat{\rho} = \rho/\rho_c$. (ii) The critical isochore $\hat{P}(\hat{\rho} = 1; \hat{T})$ is subtracted from the original EOSs, giving the shifted EOSs (Fig. 2B), $\delta\hat{P}(\hat{\rho}; \hat{T}) = \hat{P}(\hat{\rho}; \hat{T}) - \hat{P}(1; \hat{T})$. Here the critical isochore is analogous to the $H = 0$ line in the Ising model; in particular, along the critical isochore, κ_T exhibits the standard critical scaling, $\kappa_T \sim (T - T_c)^{-\gamma}$, for $T > T_c$. Thus the critical isochore above the critical point can be considered as an

extension of the coexistence line. Due to this symmetry, we take the critical isochore as the reference line to obtain shifted EOSs. Similar to the isothermal EOSs $H(m; T)$ of the Ising model, which all intersect at a point ($m = 0, H = 0$), the shifted EOSs $\delta\hat{P}(\hat{\rho}; \hat{T})$ intersect at a common point ($\hat{\rho} = 0, \delta\hat{P} = 0$). The susceptibility κ_T is the inverse slope of the shifted EOS for constant \hat{T} . The estimated κ_T is consistent with the density fluctuation data measured in scattering experiments (see SI Fig. S18 for the case of carbon dioxide). (iii) For a fixed $\delta\hat{P}$, the compressibility $\kappa_T(\hat{T}; \delta\hat{P})$ peaks at $\hat{T}_{\max}^+(\delta\hat{P})$ for $\delta\hat{P} > 0$ (see Fig. 2C) and $\hat{T}_{\max}^-(\delta\hat{P})$ for $\delta\hat{P} < 0$ (see Fig. 2D). Connecting the points $\hat{T}_{\max}^\pm(\delta\hat{P})$ together gives the two lines L^\pm (see Fig. 2B). Figure 2E shows L^\pm lines in the $\Delta\hat{P} - \Delta\hat{T}$ phase diagram, where $\Delta\hat{P} = P/P_c - 1$ and $\Delta\hat{T} = T/T_c - 1$. These two lines separate liquid-like, liquid-gas-indistinguishable and gas-like phases, which are counterparts of positive ferromagnetic-like, paramag-

netic and negative ferromagnetic-like phases in the Ising model. The described procedure applies generally to the van der Waals EOS, a standard theoretical model for gases and liquids (see SI Sec. S3), and to the experimental EOSs of other substances (e.g., water, see SI Sec. S4).

It is clear that L^\pm lines are defined according to *thermodynamics* rather than dynamics. The criterion of L^\pm is similar to that of the Widom line; the key difference is that the maxima of the response function κ_T are evaluated along paths parallel to the critical isochore (see Fig. 2E), instead of along constant-pressure or constant-temperature paths. Each parallel path that is $\delta\hat{P}$ away from the critical isochore is tangential to a constant- κ_T contour line, at the point of tangency $\hat{T}_{\max}^+(\delta\hat{P})$ or $\hat{T}_{\max}^-(\delta\hat{P})$. Note that for better visualization, in Fig. 2E we plot the color map and contour lines of constant $1/\kappa_T$, where a maximum becomes a minimum without changing its location.

Using a linear scaling theory (see SI Sec. S5) [17], we establish theoretically the scalings of L^\pm lines near the liquid-gas critical point,

$$|\delta\hat{P}^\pm| \sim (T - T_c)^{\beta+\gamma}, \quad (3)$$

and

$$|\Delta\hat{\rho}^\pm| \sim (T - T_c)^\beta, \quad (4)$$

where $\delta\hat{P}^\pm$ and $\Delta\hat{\rho}^\pm$ are values on the L^\pm lines ($\Delta\hat{\rho} = \rho/\rho_c - 1$). To verify Eqs. (3) and (4), we collect the experimental data of eight common substances, including water (H_2O), carbon dioxide (CO_2), argon (Ar), nitrogen (N), neon (Ne), propane (C_3H_8), dinitrogen monoxide (N_2O) and oxygen (O_2) from the NIST database, and evaluate their L^\pm lines using the same approach as demonstrated above for argon (Fig. 2). Figure 3 shows that both scalings are confirmed by the data of all eight substances examined, with the 3D Ising universality class exponents. Furthermore, the scalings Eqs. (3) and (4) are robust, independent of which thermodynamic response function is chosen to determine the maxima (see SI Sec. S5 and S7). Equations (1-4) recover the critical universality: the two supercritical crossover lines L^\pm obey scaling laws with the same exponents in both liquid-gas and Ising systems.

Next we compare L^\pm lines with supercritical crossovers reported previously in two sets of independent experiments (simulations) [1–3]. In the first set, *dynamical* supercritical crossovers are estimated based on the sound dispersion data obtained for supercritical argon, by inelastic X-ray scattering experiments and molecular dynamics simulations [1, 2]. From these data, sharp crossovers are determined between a regime of positive sound dispersion ratio that increases with ρ at constant T , and a regime of weak, ρ -independent sound dispersion (see SI Sec. S8). The increasing positive dispersion in the first regime reflects typical viscoelastic behavior of liquid-like states, implying the existence of two relaxation mechanisms – structural relaxations related to the so-called α -processes and microscopic relaxations related

to nearest-neighbour interactions [1, 46, 47]. In the second regime, the weak constant dispersion implies that the structural relaxations disappear and only the microscopic relaxations remain, representing non-liquid-like (gas-like or indistinguishable) states [48, 49]. In Fig. 4(A), the dynamical crossovers from sound-dispersion data are compared with L^\pm lines and previously proposed crossover lines (I–VI). Good agreement is found between the experimental dynamical crossovers and the L^+ line. Interestingly, the L^+ line is close to the Frenkel line determined by various criteria. In Fig. 4, the Frenkel-1 line is defined by the equality $\tau_0 = \tau$ between the vibration time τ_0 and the liquid relaxation time τ for the Lennard-Jones model [6], the Frenkel-2 line corresponds to the disappearance of oscillations and minima of the velocity autocorrelation function [29], and the Frenkel-3 line is derived based on isochoric heat capacity C_V (for monatomic systems such as argon, the criterion is $C_V = 2k_B$, where k_B is the Boltzmann constant) [6]. We emphasize that the Frenkel line has a dynamic nature, and it cannot satisfy the scalings Eq. (3) and (4) in the vicinity of the critical point since it does not end at the critical point (see Fig. S15). In future studies, it is of interest to understand if there is a deep connection between L^+ and Frenkel lines, which are based respectively on thermodynamic and dynamic criteria.

In the second experiment, a supercritical crossover is estimated based on the small-angle neutron scattering data of carbon dioxide [3]. The data show that, above a crossover pressure, $\hat{P}_{\text{cro}} = 1.63$ ($P_{\text{cro}} = 120$ bar) at a fixed $\hat{T} = 1.046$ ($T = 45^\circ \text{C}$), the density and density fluctuation are enhanced compared with the standard NIST data for a homogeneous state. It is expected that the formation of liquid droplets causes such enhancement; correspondingly \hat{P}_{cro} indicates a crossover to liquid-like behavior. The location of this crossover point is consistent with L^+ line, as shown in Fig. 4(B).

DISCUSSION

The above two examples demonstrate remarkable coincidences between the L^+ line and previous experimental results. The prediction of L^- line remains to be examined in future experiments. In SI Sec. S11, we show that the L^- line can be validated independently by the behavior of EOS for the compressibility factor Z above the critical temperature: the EOS of gas states can be well described by a universal form $Z_{\text{gas}}(\rho, T)$ derived from the van der Waals equation in the dilute gas limit, and the deviation points from $Z_{\text{gas}}(\rho, T)$ coincide with the L^- line. Based on the above results, the physical meaning of two supercritical crossover lines can be interpreted. The L^+ and L^- lines represent the loci in the phase diagram where the system starts to deviate from liquid and gas behavior respectively, and the indistinguishable states between the two lines behave neither like a standard liquid nor a standard gas. This study focuses on the thermodynamic

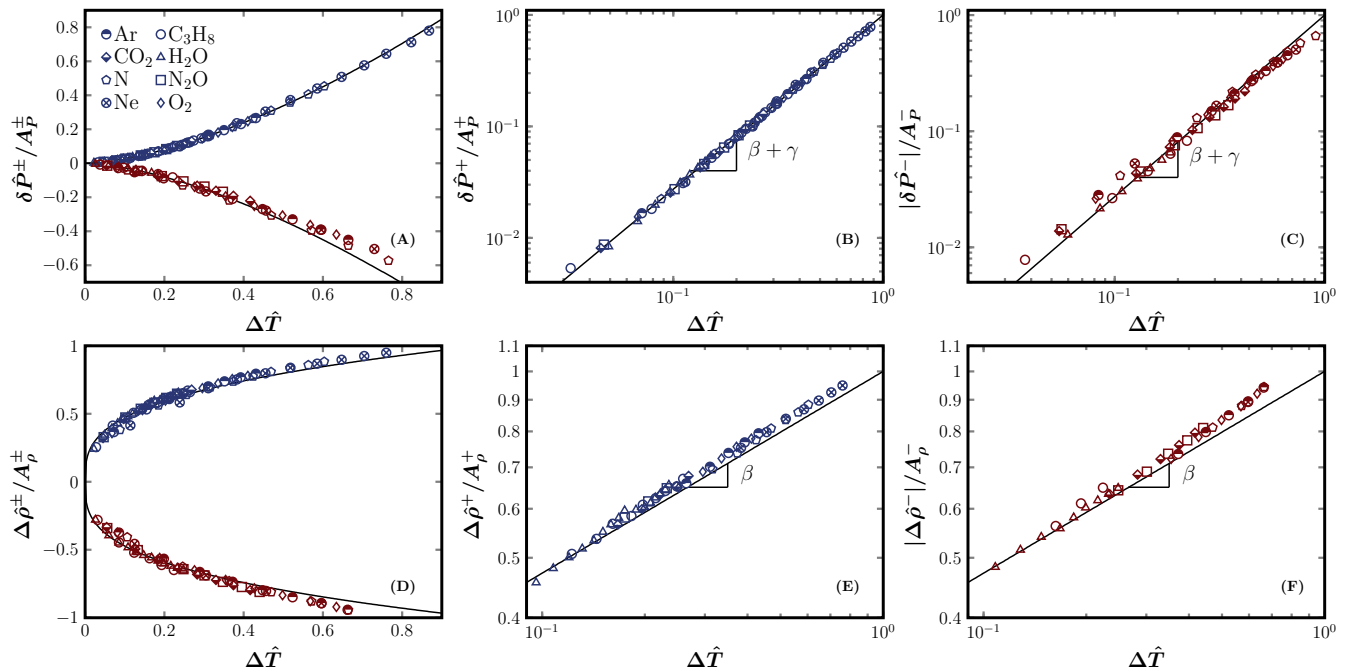


FIG. 3. **Scalings of supercritical crossover lines L^\pm near the critical point in eight substances.** (A) $\delta\hat{P}^\pm/A_P^\pm$ as a function of $\Delta\hat{T}$. The data points are fitted to $|\delta\hat{P}^\pm| = A_P^\pm \Delta\hat{T}^{\beta+\gamma}$ (solid lines), where A_P^\pm are non-universal fitting parameters (see SI Table S2 for values of A_P^\pm), and the exponents are fixed by the 3D Ising universality values, $\beta = 0.3265$ and $\gamma = 1.237$. (B) and (C) are log-log plots for L^+ and L^- respectively. (D-F) Similar plots for the scaling $|\Delta\hat{\rho}^\pm| = A_\rho^\pm \Delta\hat{T}^\beta$.

consequences of the L^+ and L^- lines. From the dynamic viewpoint, the deviation from the liquid dynamics corresponds to the Frenkel line, where the vibration motion of molecules disappears. As shown in Fig. 4A, the L^+ and Frenkel lines are indeed close to each other. The deviation from the gas dynamics has not been considered previously; it will be interesting to investigate how the dynamics change around the L^- line in the future.

Finally, it should be straightforward to generalize the present analysis to other phase transitions, including liquid-liquid phase transitions [4], quantum phase transitions [54], non-equilibrium phase transitions such as liquid-glass transitions [55], and phase transitions in dusty plasmas [56]. In particular, recent studies [54, 57–59] have revealed the analogy between the critical point of water and that of certain quantum magnetic systems, where two supercritical crossover lines can be determined according to the behavior of specific heat. It is expected that the L^\pm lines in such quantum magnetic

systems can be defined following the method provided here, which should obey the same universal scalings as Eqs. (3) and (4), independent of the slope of the coexistence line (see SI Sec. S5) and of which thermodynamic response function is chosen to determine L^\pm (see SI Sec. S5 and S7B).

ACKNOWLEDGMENTS

We thank Limei Xu, Matteo Baggioli, Yan Feng, Xinzheng Li, Haijun Zhou, Chengran Du, Jie Zhang, Rui Shi and Chong Zha for discussions. We acknowledge financial support from NSFC (Grants 11935002, 11974361, 12161141007 and 12047503), from Chinese Academy of Sciences (Grants ZDBS-LY-7017 and KGFZD-145-22-13), and from Wenzhou Institute (Grant WIUCA-SICTP2022). In this work access was granted to the High-Performance Computing Cluster of Institute of Theoretical Physics - the Chinese Academy of Sciences.

-
- [1] G. Simeoni, T. Bryk, F. Gorelli, M. Krisch, G. Ruocco, M. Santoro, and T. Scopigno, The widom line as the crossover between liquid-like and gas-like behaviour in supercritical fluids, *Nature Physics* **6**, 503 (2010).
 [2] F. Gorelli, T. Bryk, M. Krisch, G. Ruocco, M. Santoro, and T. Scopigno, Dynamics and thermodynamics beyond the critical point, *Scientific Reports* **3**, 1 (2013).

- [3] V. Pipich and D. Schwahn, Densification of supercritical carbon dioxide accompanied by droplet formation when passing the widom line, *Physical review letters* **120**, 145701 (2018).
 [4] L. Xu, P. Kumar, S. V. Buldyrev, S.-H. Chen, P. H. Poole, F. Sciortino, and H. E. Stanley, Relation between the widom line and the dynamic crossover in systems

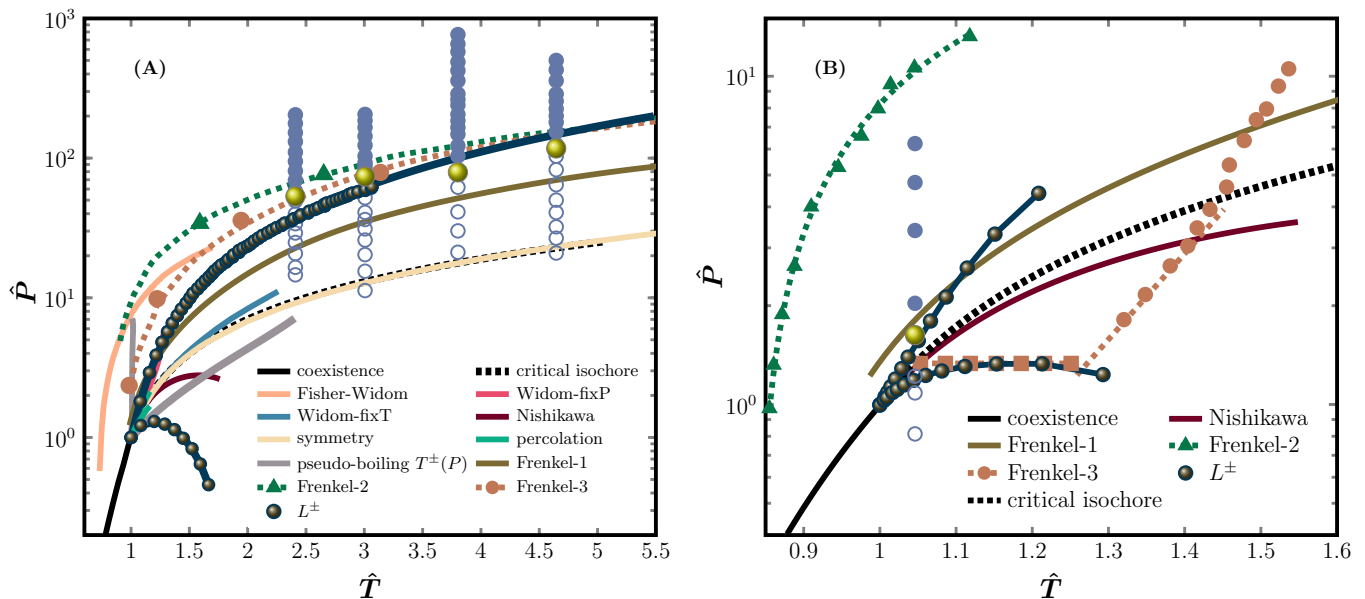


FIG. 4. **Comparison between supercritical crossover lines and experimental (simulation) data.** (A) \hat{P} - \hat{T} diagram of supercritical argon. The data points of L^\pm lines are obtained in Fig. 2, and fitted to the scaling form Eq. (3) (solid lines, see SI Sec. S7 for a discussion on the fitting). Filled and open blue circles are data points collected from [1, 2] at four different \hat{T} : the filled circles are with positive increasing sound dispersion, and the open circles are with weak constant sound dispersion; they are separated by crossover points indicated by yellow balls (see SI Sec. S8). The Fisher-Widom line [50], Frenkel-1 line [6], Frenkel-2 line [29], Frenkel-3 line [6], symmetry line [8] and percolation lines [9] are copied from the cited publications correspondingly. The Nishikawa line is evaluated in SI Sec. S10 according to its definition. The Widom lines are determined based on the NIST EOSs, for fixed P and fixed T . The pseudo-boiling boundaries $T^\pm(P)$ are determined following the definition given in [15]. An enlarged view near the critical point is provided in Fig. S15. (B) \hat{P} - \hat{T} diagram of supercritical carbon dioxide. Filled and open blue circles are data points collected from [3]: the filled/open circles are with/without enhanced density fluctuations compared to the NIST data, separated by the crossover point (yellow ball). The Frenkel-1 line [6], Frenkel-2 line [51], Frenkel-3 line (defined at $C_V = 3.5k_B$ for carbon dioxide) [3, 52], and Nishikawa line [53] are copied from the cited publications correspondingly.

with a liquid–liquid phase transition, Proceedings of the National Academy of Sciences **102**, 16558 (2005).

- [5] M. E. Fisher and B. Widom, Decay of correlations in linear systems, The Journal of Chemical Physics **50**, 3756 (1969).
- [6] V. Brazhkin, Y. D. Fomin, A. Lyapin, V. Ryzhov, and K. Trachenko, Two liquid states of matter: A dynamic line on a phase diagram, Physical Review E **85**, 031203 (2012).
- [7] K. Nishikawa and I. Tanaka, Correlation lengths and density fluctuations in supercritical states of carbon dioxide, Chemical physics letters **244**, 149 (1995).
- [8] E. A. Ploetz and P. E. Smith, Gas or liquid? the supercritical behavior of pure fluids, The Journal of Physical Chemistry B **123**, 6554 (2019).
- [9] L. V. Woodcock, Observations of a thermodynamic liquid–gas critical coexistence line and supercritical fluid phase bounds from percolation transition loci, Fluid Phase Equilibria **351**, 25 (2013).
- [10] S. E. Strong, L. Shi, and J. Skinner, Percolation in supercritical water: Do the widom and percolation lines coincide?, The Journal of chemical physics **149**, 084504 (2018).
- [11] Nist chemistry webbook, <http://webbook.nist.gov/chemistry/>.
- [12] G. Jones and P. Walker, Specific heats of fluid argon near the critical point, Proceedings of the Physical Society. Section B **69**, 1348 (1956).
- [13] V. Brazhkin, Y. D. Fomin, A. Lyapin, V. Ryzhov, and E. Tsiok, Widom line for the liquid–gas transition in lennard-jones system, The Journal of Physical Chemistry B **115**, 14112 (2011).
- [14] G. Ruppeiner, A. Sahay, T. Sarkar, and G. Sengupta, Thermodynamic geometry, phase transitions, and the widom line, Physical Review E **86**, 052103 (2012).
- [15] D. Banuti, Crossing the widom-line–supercritical pseudo-boiling, The Journal of Supercritical Fluids **98**, 12 (2015).
- [16] H.-O. May and P. Mausbach, Riemannian geometry study of vapor-liquid phase equilibria and supercritical behavior of the lennard-jones fluid, Physical Review E **85**, 031201 (2012).
- [17] J. Luo, L. Xu, E. Lascaris, H. E. Stanley, and S. V. Buldyrev, Behavior of the widom line in critical phenomena, Physical Review Letters **112**, 135701 (2014).
- [18] D. Banuti, M. Raju, and M. Ihme, Similarity law for widom lines and coexistence lines, Physical Review E **95**, 052120 (2017).
- [19] D. Corradini, M. Rovere, and P. Gallo, The widom line and dynamical crossover in supercritical water: Popular water models versus experiments, The Journal of Chemical Physics **143**, 114502 (2015).
- [20] P. Gallo, D. Corradini, and M. Rovere, Widom line and

- dynamical crossovers as routes to understand supercritical water, *Nature communications* **5**, 1 (2014).
- [21] E. de Jesús, J. Torres-Arenas, and A. Benavides, Widom line of real substances, *Journal of Molecular Liquids* **322**, 114529 (2021).
- [22] R. L. De Carvalho, R. Evans, D. Hoyle, and J. Henderson, The decay of the pair correlation function in simple fluids: long-versus short-ranged potentials, *Journal of Physics: Condensed Matter* **6**, 9275 (1994).
- [23] C. Vega, L. Rull, and S. Lago, Location of the fisher-widom line for systems interacting through short-ranged potentials, *Physical Review E* **51**, 3146 (1995).
- [24] M. Dijkstra and R. Evans, A simulation study of the decay of the pair correlation function in simple fluids, *The Journal of Chemical Physics* **112**, 1449 (2000).
- [25] R. Evans, J. Henderson, D. Hoyle, A. Parry, and Z. Sabeur, Asymptotic decay of liquid structure: oscillatory liquid-vapour density profiles and the fisher-widom line, *Molecular Physics* **80**, 755 (1993).
- [26] P. Tarazona, E. Chacón, and E. Velasco, The fisher-widom line for systems with low melting temperature, *Molecular Physics* **101**, 1595 (2003).
- [27] D. Stopper, H. Hansen-Goos, R. Roth, and R. Evans, On the decay of the pair correlation function and the line of vanishing excess isothermal compressibility in simple fluids, *The Journal of chemical physics* **151**, 014501 (2019).
- [28] T. J. Yoon, M. Y. Ha, W. B. Lee, and Y.-W. Lee, “two-phase” thermodynamics of the frenkel line, *The journal of physical chemistry letters* **9**, 4550 (2018).
- [29] V. Brazhkin, Y. D. Fomin, A. Lyapin, V. Ryzhov, E. Tsiok, and K. Trachenko, “liquid-gas” transition in the supercritical region: Fundamental changes in the particle dynamics, *Physical review letters* **111**, 145901 (2013).
- [30] D. Bolmatov, V. Brazhkin, and K. Trachenko, Thermodynamic behaviour of supercritical matter, *Nature communications* **4**, 1 (2013).
- [31] D. Bolmatov, D. Zav’yalov, M. Gao, and M. Zhernenkov, Structural evolution of supercritical CO_2 across the frenkel line, *The journal of physical chemistry letters* **5**, 2785 (2014).
- [32] C. Prescher, Y. D. Fomin, V. Prakapenka, J. Stefanski, K. Trachenko, and V. Brazhkin, Experimental evidence of the frenkel line in supercritical neon, *Physical Review B* **95**, 134114 (2017).
- [33] D. Bolmatov, M. Zhernenkov, D. Zav’yalov, S. N. Tkachev, A. Cunsolo, and Y. Q. Cai, The frenkel line: a direct experimental evidence for the new thermodynamic boundary, *Scientific reports* **5**, 1 (2015).
- [34] Y. D. Fomin, V. Ryzhov, E. Tsiok, J. Proctor, C. Prescher, V. Prakapenka, K. Trachenko, and V. Brazhkin, Dynamics, thermodynamics and structure of liquids and supercritical fluids: crossover at the frenkel line, *Journal of Physics: Condensed Matter* **30**, 134003 (2018).
- [35] J. Proctor, C. Pruteanu, I. Morrison, I. Crowe, and J. Loveday, Transition from gas-like to liquid-like behavior in supercritical N_2 , *The Journal of Physical Chemistry Letters* **10**, 6584 (2019).
- [36] Y. D. Fomin, V. Ryzhov, E. Tsiok, and V. Brazhkin, Dynamical crossover line in supercritical water, *Scientific reports* **5**, 1 (2015).
- [37] V. V. Brazhkin, Y. D. Fomin, A. G. Lyapin, V. N. Ryzhov, and K. Trachenko, Universal crossover of liquid dynamics in supercritical region, *JETP letters* **95**, 164 (2012).
- [38] C. Cockrell, V. V. Brazhkin, and K. Trachenko, Transition in the supercritical state of matter: Review of experimental evidence, *Physics Reports* **941**, 1 (2021).
- [39] K. Nishikawa and T. Morita, Fluid behavior at supercritical states studied by small-angle x-ray scattering, *The Journal of supercritical fluids* **13**, 143 (1998).
- [40] M. Matsugami, N. Yoshida, and F. Hirata, Theoretical characterization of the “ridge” in the supercritical region in the fluid phase diagram of water, *The Journal of Chemical Physics* **140**, 104511 (2014).
- [41] L. V. Woodcock, Thermodynamics of gas–liquid criticality: rigidity symmetry on gibbs density surface, *International Journal of Thermophysics* **37**, 1 (2016).
- [42] F. Maxim, K. Karalis, P. Boillat, D. T. Banuti, J. I. Marquez Damian, B. Niceno, and C. Ludwig, Thermodynamics and dynamics of supercritical water pseudo-boiling, *Advanced Science* **8**, 2002312 (2021).
- [43] L. P. Kadanoff, Scaling, universality and operator algebras, in *Phase Transitions and Critical Phenomena*, Vol. 5A, edited by C. Domb and M. S. Green (Academic, New York, 1976) Chap. 1.
- [44] M. E. Fisher, Scaling, universality and renormalization group theory, in *Critical phenomena* (Springer, 1983) pp. 1–139.
- [45] R. Guida and J. Zinn-Justin, Critical exponents of the n-vector model, *Journal of Physics A: Mathematical and General* **31**, 8103 (1998).
- [46] F. Gorelli, M. Santoro, T. Scopigno, M. Krisch, and G. Ruocco, Liquidlike behavior of supercritical fluids, *Physical review letters* **97**, 245702 (2006).
- [47] F. Bencivenga, A. Cunsolo, M. Krisch, G. Monaco, G. Ruocco, and F. Sette, Adiabatic and isothermal sound waves: The case of supercritical nitrogen, *EPL (Europhysics Letters)* **75**, 70 (2006).
- [48] G. Ruocco, F. Sette, R. Di Leonardo, G. Monaco, M. Sampoli, T. Scopigno, and G. Viliani, Relaxation processes in harmonic glasses?, *Physical Review Letters* **84**, 5788 (2000).
- [49] T. Scopigno, G. Ruocco, F. Sette, and G. Viliani, Evidence of short-time dynamical correlations in simple liquids, *Physical Review E* **66**, 031205 (2002).
- [50] P. Gallo, K. Amann-Winkel, C. A. Angell, M. A. Anisimov, F. Caupin, C. Chakravarty, E. Lascaris, T. Loerting, A. Z. Panagiotopoulos, J. Russo, *et al.*, Water: A tale of two liquids, *Chemical reviews* **116**, 7463 (2016).
- [51] C. Yang, V. Brazhkin, M. Dove, and K. Trachenko, Frenkel line and solubility maximum in supercritical fluids, *Physical Review E* **91**, 012112 (2015).
- [52] Y. D. Fomin, V. Ryzhov, E. Tsiok, and V. Brazhkin, Thermodynamic properties of supercritical carbon dioxide: Widom and frenkel lines, *Physical Review E* **91**, 022111 (2015).
- [53] A. Imre, C. Ramboz, U. K. Deiters, and T. Kraska, Anomalous fluid properties of carbon dioxide in the supercritical region: Application to geological CO_2 storage and related hazards, *Environmental Earth Sciences* **73**, 4373 (2015).
- [54] J. L. Jiménez, S. Crone, E. Fogh, M. E. Zayed, R. Lortz, E. Pomjakushina, K. Conder, A. M. Läuchli, L. Weber, S. Wessel, *et al.*, A quantum magnetic analogue to the critical point of water, *Nature* **592**, 370 (2021).
- [55] L. Berthier and R. L. Jack, Evidence for a disordered critical point in a glass-forming liquid, *Physical review*

- letters **114**, 205701 (2015).
- [56] D. Huang, M. Baggioli, S. Lu, Z. Ma, and Y. Feng, Revealing the supercritical dynamics of dusty plasmas and their liquidlike to gaslike dynamical crossover, *Physical Review Research* **5**, 013149 (2023).
- [57] J. Stappmanns, P. Corboz, F. Mila, A. Honecker, B. Normand, and S. Wessel, Thermal critical points and quantum critical end point in the frustrated bilayer heisenberg antiferromagnet, *Physical Review Letters* **121**, 127201 (2018).
- [58] L. Weber, A. Honecker, B. Normand, P. Corboz, F. Mila, and S. Wessel, Quantum monte carlo simulations in the trimer basis: first-order transitions and thermal critical points in frustrated trilayer magnets, *SciPost Physics* **12**, 054 (2022).
- [59] J. Wang, H. Li, N. Xi, Y. Gao, Q.-B. Yan, W. Li, and G. Su, Plaquette singlet transition, magnetic barocaloric effect, and spin supersolidity in the shastry-sutherland model, *Physical Review Letters* **131**, 116702 (2023).
- [60] S. G. BRUSH, History of the lenz-ising model, *Rev. Mod. Phys.* **39**, 883 (1967).
- [61] R. J. Baxter, *Exactly solved models in statistical mechanics* (Elsevier, 2016).
- [62] U. Wolff, Collective monte carlo updating for spin systems, *Physical Review Letters* **62**, 361 (1989).
- [63] M. E. Newman and G. T. Barkema, *Monte Carlo methods in statistical physics* (Clarendon Press, 1999).
- [64] M. E. Fisher and R. J. Burford, Theory of critical-point scattering and correlations. i. the ising model, *Physical Review* **156**, 583 (1967).
- [65] O. Mishima and H. E. Stanley, The relationship between liquid, supercooled and glassy water, *Nature* **396**, 329 (1998).
- [66] A. G. Smart, The war over supercooled water, *Physics Today* **22** (2018).
- [67] K. H. Kim, A. Späh, H. Pathak, F. Perakis, D. Mariedahl, K. Amann-Winkel, J. A. Sellberg, J. H. Lee, S. Kim, J. Park, *et al.*, Maxima in the thermodynamic response and correlation functions of deeply supercooled water, *Science* **358**, 1589 (2017).
- [68] M. F. Chaplin, Structure and properties of water in its various states, *Encyclopedia of water: science, technology, and society*, 1 (2019).
- [69] B. Widom, Equation of state in the neighborhood of the critical point, *The Journal of Chemical Physics* **43**, 3898 (1965).
- [70] B. Widom, The critical point and scaling theory, *Physica* **73**, 107 (1974).
- [71] M. Anisimov, V. Agayan, and P. J. Collings, Nature of the blue-phase-iii–isotropic critical point: an analogy with the liquid-gas transition, *Physical Review E* **57**, 582 (1998).
- [72] D. Fuentesvilla and M. Anisimov, Scaled equation of state for supercooled water near the liquid-liquid critical point, *Physical review letters* **97**, 195702 (2006).
- [73] P. Schofield, Parametric representation of the equation of state near a critical point, *Physical Review Letters* **22**, 606 (1969).
- [74] P. Schofield, J. Litster, and J. T. Ho, Correlation between critical coefficients and critical exponents, *Physical Review Letters* **23**, 1098 (1969).
- [75] Y. C. Kim, M. A. Anisimov, J. V. Sengers, and E. Luijten, Crossover critical behavior in the three-dimensional ising model, *Journal of statistical physics* **110**, 591 (2003).
- [76] K. Nishikawa, K. Kusano, A. Ayusawa Arai, and T. Morita, Density fluctuation of a van der waals fluid in supercritical state, *The Journal of chemical physics* **118**, 1341 (2003).

Supplementary Information

CONTENTS

Methods and Results	3
Discussion	4
Acknowledgments	5
References	5
S1. Ising model	9
A. Mean-field theory	10
B. Monte Carlo simulations in two and three dimensions	11
S2. Summary of supercritical crossover lines in the literature	11
S3. van der Waals equation of state	13
A. Determination of L^\pm lines	13
B. L^\pm lines in pressure-temperature and pressure-volume phase diagrams	14
S4. L^\pm lines of water	14
S5. Linear scaling theory	15
A. Sketch of the theory	15
B. Symmetric model with $\varphi = 0$	17
C. Asymmetric models with $\varphi \neq 0$	17
S6. Summary of the coefficients A_p^\pm and A_ρ^\pm in Fig.3.	18
S7. Additional data of L^\pm lines of argon	19
A. Examination of different fitting methods	19
B. L^\pm lines defined by different response functions	19
S8. Reestimation of dynamical crossovers in supercritical argon from sound dispersion data	21
S9. Comparison of different supercritical crossover lines of argon in the vicinity of the critical point	22
S10. Nishikawa line of argon	22
S11. Validation of L^- line by the equation of states for the compressibility factor	22
S12. Comparison between density fluctuations estimated from NIST EOSs and those measured in scattering experiments	24

S1. ISING MODEL

The Hamiltonian of the Ising model is [60],

$$\mathcal{H} = -J \sum_{\langle i,j \rangle} s_i s_j - H \sum_{i=1}^N s_i, \quad (\text{S1})$$

where J is a coupling constant, $s_i = \pm 1$ the value of spin on the i -th site, N the total number of spins, H the external magnetic field, and $\langle i, j \rangle$ stands for nearest-neighbor spin pairs. The model is defined on a square lattice in d dimensions. The mean magnetization is $m = \frac{1}{N} \left\langle \sum_{i=1}^N s_i \right\rangle$, where $\langle \dots \rangle$ is the ensemble average, and the susceptibility is $\chi = \left(\frac{\partial m}{\partial H} \right)_T$.

According to the definition, on the supercritical ($T > T_c$) crossover lines L^\pm , χ is maximum, i.e.,

$$\left(\frac{\partial\chi}{\partial T}\right)_H = 0, \quad (\text{S2})$$

where T_c is the critical temperature. The purpose of this section is to show that on L^\pm the order parameter m^\pm and the field H^\pm satisfy two scalings, Eqs. (1) and (2), near the critical point. We first derive these two scalings analytically from a mean-field calculation, and then demonstrate that they also hold in two and three dimensions ($d = 2$ and 3) using Monte Carlo simulations.

A. Mean-field theory

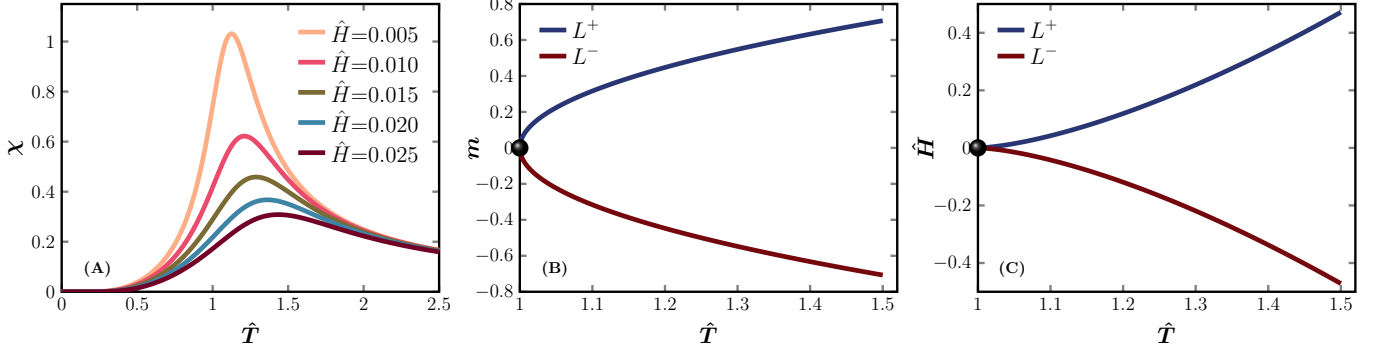


FIG. S1. **Supercritical crossover lines L^\pm in the mean-field Ising model.** (A) Magnetic susceptibility χ as a function of the reduced temperature \hat{T} , for a few different reduced magnetic fields \hat{H} . The peaks determine the supercritical crossover lines L^\pm . Along L^\pm , (B) m^\pm changes with \hat{T} following Eq. (S8), and (C) \hat{H}^\pm changes with \hat{T} following Eqs. (S9).

With the mean-field approximation, m and χ are easy to calculate [61]:

$$m = \tanh[\beta(H + qJm)], \quad (\text{S3})$$

and

$$\chi = \frac{\beta}{\cosh^2[\beta(H + qJm)] - \beta Jq}, \quad (\text{S4})$$

where $q = 2d$ is the coordination number (i.e., the number of nearest neighbors of each spin), and $\beta = 1/k_B T$ the inverse temperature. We set the Boltzmann constant $k_B = 1$.

In the following derivations, we switch to the reduced parameters $\hat{H} = H/T_c$ and $\hat{T} = T/T_c$, where $T_c = qJ$. With the reduced parameters, Eq. (S3) becomes,

$$\begin{aligned} m &= \tanh\left[\frac{(\hat{H} + m)}{\hat{T}}\right] \\ &\approx \frac{\hat{H} + m}{\hat{T}} - \frac{1}{3}\left(\frac{\hat{H} + m}{\hat{T}}\right)^3, \end{aligned} \quad (\text{S5})$$

where we have expanded it up to the third order, assuming that \hat{H} and m are small near the critical point. Defining $\hat{\chi} = T_c \chi$, from Eq. (S5) we obtain,

$$\hat{\chi} = \left(\frac{\partial m}{\partial \hat{H}}\right)_{\hat{T}} = \frac{1 - (\hat{H} + m)^2/\hat{T}^2}{\hat{T} - 1 + (\hat{H} + m)^2/\hat{T}^2}. \quad (\text{S6})$$

Making a change of variable $A = (\hat{H} + m)/\hat{T}$, and taking the partial derivative of Eq. (S6) with respect to the temperature, we get

$$\left(\frac{\partial \hat{\chi}}{\partial \hat{T}}\right)_{\hat{H}} = \frac{(3A^2 - 1)(\hat{T} - 1 + A^2) + 2A^2(1 - A^2)}{(\hat{T} - 1 + A^2)^3}, \quad (\text{S7})$$

which should be 0 on the L^\pm . The solution of $\left(\frac{\partial \chi}{\partial \hat{T}}\right)_{\hat{H}} = 0$ is, $(A^\pm)^2 = \hat{T} - 1$, or,

$$|m^\pm| = (\hat{T} - 1)^{1/2}, \quad (\text{S8})$$

near the critical point, where the exponent is equal to the mean-field exponent $\beta = 1/2$ (note that $|\hat{H}^\pm|$ is higher order; see Eq. S9). Equation (S8) gives the scaling relationship between the order parameter and temperature on L^\pm (see Fig. S1). Using Eq. (S5), we can convert Eq. (S8) into a relationship between the external field \hat{H}^\pm and \hat{T} on L^\pm ,

$$|\hat{H}^\pm| = \frac{4}{3} (\hat{T} - 1)^{3/2}, \quad (\text{S9})$$

where the exponent is equal to $\beta + \gamma = 3/2$ with the mean-field exponents $\beta = 1/2$ and $\gamma = 1$. The mean-field scalings are plotted in Fig. S1.

Equations (S8) and (S9) are the mean-field form of scalings Eqs. (1) and (2). In Sec. S5, we will derive these scalings using a general linear scaling theory without the mean-field approximation.

B. Monte Carlo simulations in two and three dimensions

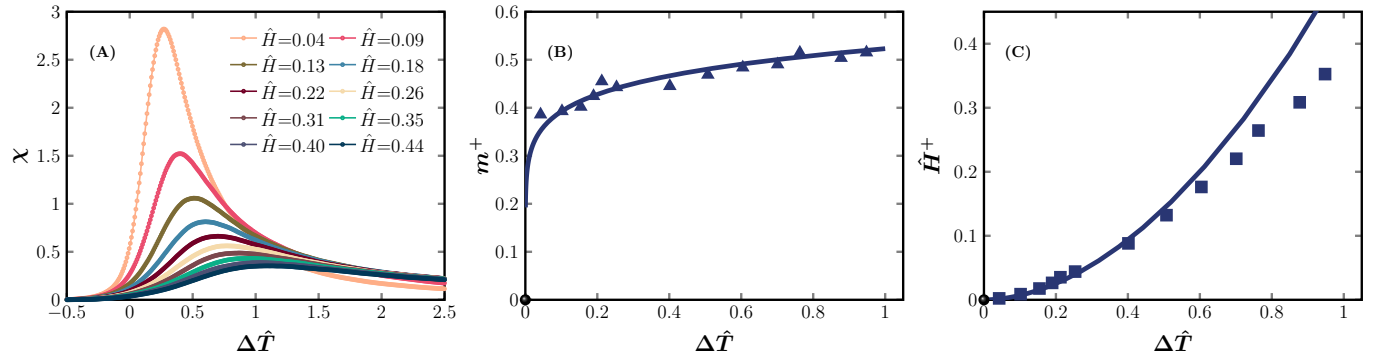


FIG. S2. **Supercritical crossover lines L^\pm in the 2D Ising model.** Results are obtained from Monte Carlo simulations. (A) Magnetic susceptibility χ as a function of the reduced temperature \hat{T} , for a few different reduced magnetic fields \hat{H} . The peaks determine the supercritical crossover line L^+ (the L^- line is symmetric to the L^+ line and not shown). (B) The magnetization m^+ and (C) reduced field \hat{H}^+ along the L^+ line are plotted as functions of $\Delta \hat{T}$. The lines represent fits, $m^+ = A_m \Delta \hat{T}^\beta$ and $\hat{H}^+ = A_H \Delta \hat{T}^{\beta+\gamma}$, where $A_m = 0.523$ and $A_H = 0.521$ are fitting parameters (see Fig. S3 for corresponding log-log plots).

We study the Ising model in both two (2D) and three (3D) dimensions to validate the scaling relationships Eqs. (1) and (2), using Monte Carlo simulations with the wolff algorithm [62, 63]. The lattice size is 40×40 in 2D and $25 \times 25 \times 25$ in 3D. The mean magnetization is computed using the definition, $m = \frac{1}{N} \langle \sum_{i=1}^N s_i \rangle$, and the magnetic susceptibility is computed using,

$$\chi = \left(\frac{\partial m}{\partial H}\right)_T = \beta N (\langle m^2 \rangle - \langle m \rangle^2). \quad (\text{S10})$$

In simulations, m and χ are obtained by averaging over 10^4 independent equilibrium configurations. For a few given \hat{H} , the magnetic susceptibility χ is plotted as a function of temperature \hat{T} in Fig. S2(A) and Fig. S4(A), from which the peaks are located. The supercritical crossover lines determined in this way can be well fitted to scalings Eqs. (1) and (2), as shown in Figs. S2-S5. In the fitting, the exponents are fixed to the known values: $\beta = 1/8$, $\gamma = 7/4$ in 2D [64], and $\beta = 0.326$, $\gamma = 1.237$ in 3D [45]; the prefactor is treated as a fitting parameter.

S2. SUMMARY OF SUPERCritical CROSSOVER LINES IN THE LITERATURE

Table S1 summarizes supercritical crossover lines existing in the literature, compared to the proposal of this study.

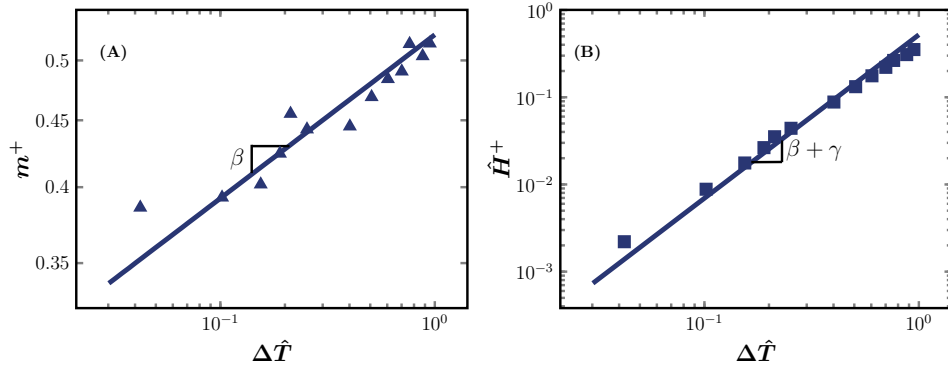


FIG. S3. **Scaling laws of the L^+ line in the 2D Ising model.** (A) The magnetization m^+ and (B) reduced field \hat{H}^+ as functions of $\Delta\hat{T}$, in log-log scales. The lines represent fits, $m^+ = A_m \Delta\hat{T}^\beta$ and $\hat{H}^+ = A_H \Delta\hat{T}^{\beta+\gamma}$, where $A_m = 0.523$ and $A_H = 0.521$ are fitting parameters.

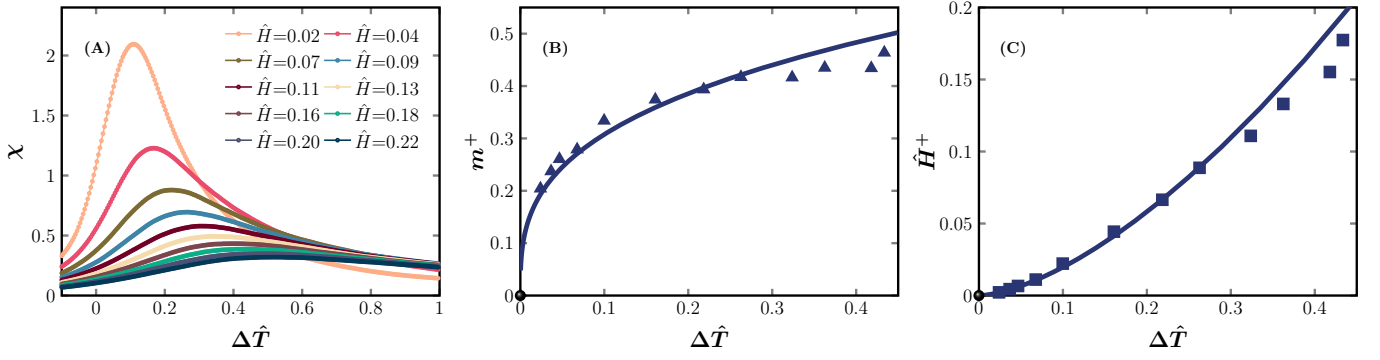


FIG. S4. **Supercritical crossover lines L^\pm in the 3D Ising model.** Results are obtained from Monte Carlo simulations. (A) Magnetic susceptibility χ as a function of the reduced temperature \hat{T} (for this panel the lattice size is $12 \times 12 \times 12$), for a few different reduced magnetic fields \hat{H} . The peaks determine the supercritical crossover line L^+ . (B) The magnetization m^+ and (C) reduced field \hat{H}^+ along the L^+ line are plotted as functions of $\Delta\hat{T}$. The lines represent fits, $m^+ = A_m \Delta\hat{T}^\beta$ and $\hat{H}^+ = A_H \Delta\hat{T}^{\beta+\gamma}$, where $A_m = 0.652$ and $A_H = 0.719$ are fitting parameters (see Fig. S5 for corresponding log-log plots).

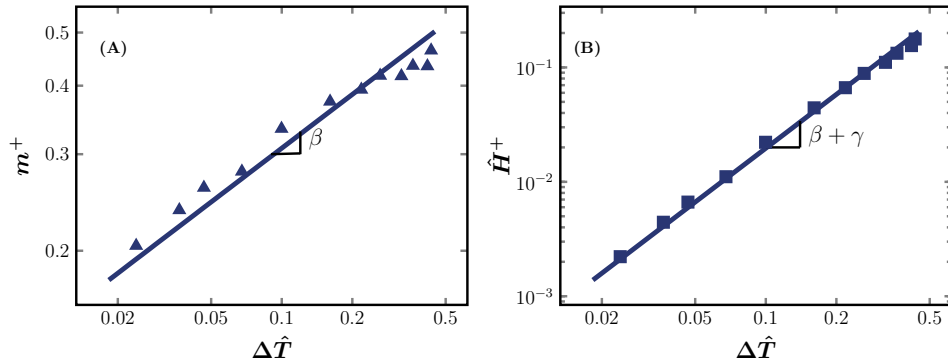


FIG. S5. **Scaling laws of the L^+ line in the 3D Ising model.** (A) The magnetization m^+ and (B) reduced field \hat{H}^+ as functions of $\Delta\hat{T}$, in log-log scales. The lines represent fits, $m^+ = A_m \Delta\hat{T}^\beta$ and $\hat{H}^+ = A_H \Delta\hat{T}^{\beta+\gamma}$, where $A_m = 0.652$ and $A_H = 0.719$ are fitting parameters.

TABLE S1. Summary of crossover lines in supercritical fluids.

crossover lines	number of lines emanating from the critical point?	obeying critical scalings Eq.(3) and (4)?	
1. Widom line [4]	one	yes	no
2. Fisher-Widom line [5]	one	no	no
3. Frenkel line [6]	one	no	no
4. Nishikawa line [7]	one	yes	no
5. symmetry line [8]	one	yes	no
6. percolation lines [9]	two	no	no
7. pseudo-boiling boundaries [15]	two	yes	no
8. L^\pm lines (this study)	two	yes	yes

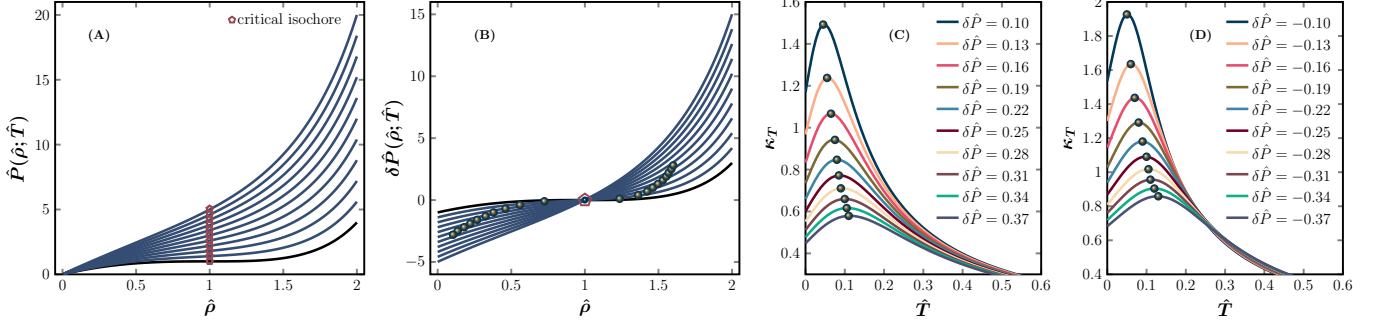


FIG. S6. **Determination of crossover lines L^\pm of the van der Waals equation of state.** (A) Isothermal EOSs, $\hat{P}(\hat{\rho}; \hat{T})$, above the critical temperature. The black line is critical isotherm, and dark blue lines are other isotherms (from bottom to top, $\hat{T} = 1.00, 1.10, 1.20, 1.30, 1.40, 1.50, 1.60, 1.70, 1.80, 1.90, 2.00$). The critical isochore is marked by pentagons. (B) Shifted EOSs $\delta\hat{P}(\hat{\rho}; \hat{T})$. The Susceptibility $\kappa_T = \left(\frac{\partial\hat{\rho}}{\partial\hat{P}}\right)_{\hat{T}}$ is plotted as a function of \hat{T} , for a few fixed (C) $\delta\hat{P} > 0$ and (D) $\delta\hat{P} < 0$; the loci of peaks determine L^+ and L^- respectively (circles). The meanings of symbols are the same in all panels.

S3. VAN DER WAALS EQUATION OF STATE

The van der Waals equation is one of the most widely used equation of state (EOS) for describing the liquid-gas phase transition. The reduced form of the van der Waals equation is,

$$\left(\hat{P} + \frac{3}{\hat{V}^2}\right)(3\hat{V} - 1) = 8\hat{T}, \quad (\text{S11})$$

where $\hat{P} = P/P_c$, $\hat{V} = V/V_c$ and $\hat{T} = T/T_c$ are the reduced pressure, volume and temperature respectively, and P_c , V_c and T_c are the pressure, volume and temperature of the critical point.

A. Determination of L^\pm lines

The supercritical crossover lines L^\pm are obtained numerically following the procedure described below. A similar procedure is used to obtain L^\pm of argon in the main text (see Fig. 2).

- Plot the isothermal EOSs $\hat{P}(\hat{\rho}; \hat{T})$ above the critical temperature, where $\hat{\rho} = 1/\hat{V}$ is the reduced density (see Fig. S6(A)).
- Subtract the critical isochore $\hat{P}(1; \hat{T})$ from the original EOS $\hat{P}(\hat{\rho}; \hat{T})$. In the shifted EOSs, $\delta\hat{P}(\hat{\rho}; \hat{T}) = \hat{P}(\hat{\rho}; \hat{T}) - \hat{P}(1; \hat{T})$, the critical isochore line $\hat{P}(1; \hat{T})$ becomes a single point $\delta\hat{P}(1; \hat{T}) = 0$ that coincides with the critical point (see Fig. S6(B)). All shifted EOSs $\delta\hat{P}(\hat{\rho}; \hat{T})$ intersect at this point.
- Along constant- $\delta\hat{P}$ paths, find the maxima of the susceptibility $\kappa_T = \left(\frac{\partial\hat{\rho}}{\partial(\delta\hat{P})}\right)_{\hat{T}}$, which give L^\pm (see Fig. S6(C) and (D)). The constant- $\delta\hat{P}$ paths correspond to lines parallel to the the critical isochore in the $\hat{P} - \hat{T}$ phase diagram.

B. L^\pm lines in pressure-temperature and pressure-volume phase diagrams

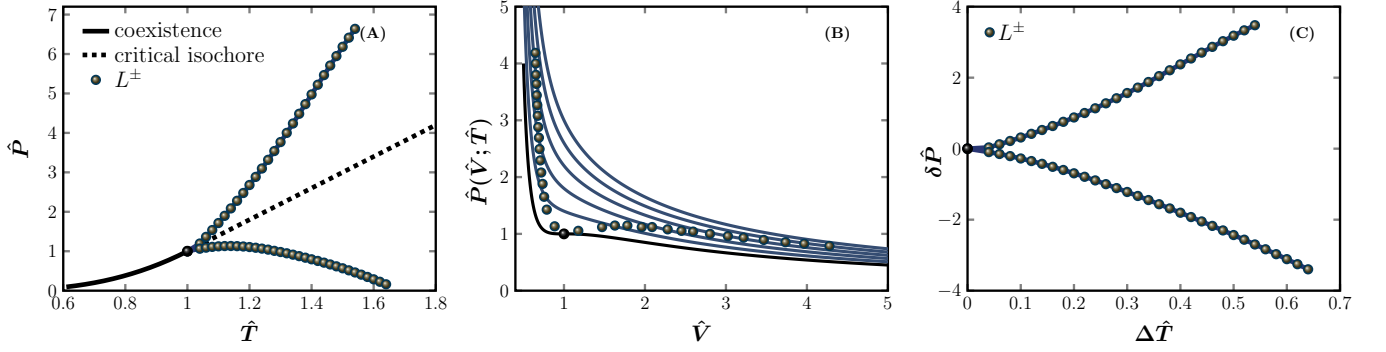


FIG. S7. **Crossover lines L^\pm of the van der Waals equation of state.** (A) Pressure-temperature ($\hat{P} - \hat{T}$) diagram. (B) Pressure-volume ($\hat{P} - \hat{V}$) diagram, where the lines are isotherms for $\hat{T} = 1.00, 1.10, 1.20, 1.30, 1.40, 1.50$. (from bottom to top). (C) $\delta\hat{P} - \Delta\hat{T}$ diagram.

The above determined crossover lines L^\pm are plotted in pressure-temperature ($\hat{P} - \hat{T}$) and pressure-volume ($\hat{P} - \hat{V}$) diagrams (see Fig. S7(A) and Fig. S7(B)). In the $\delta\hat{P} - \Delta\hat{T}$ diagram, L^+ is nearly symmetric to L^- (see Fig. S7(C)), similar to the case of Ising model (see Fig. S1A).

S4. L^\pm LINES OF WATER

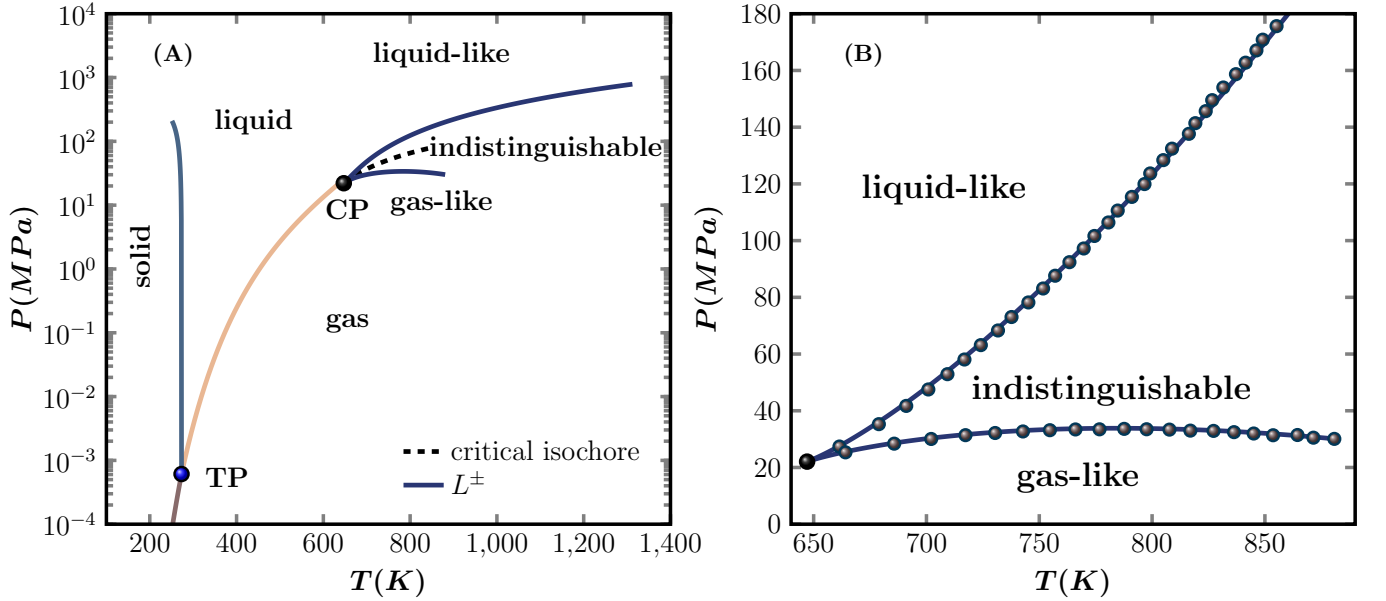


FIG. S8. **Supercritical crossover lines L^\pm of water.** (A) Pressure-temperature phase diagram of water. L^\pm lines have been included in the diagram, separating liquid-like, indistinguishable and gas-like regimes. The triple point (TP) and critical point (CP) are also indicated. (B) L^\pm lines in the vicinity of the critical point. Points are determined from the maximum of κ_T . Lines represent fitting to the data points, following the second fitting method explained in Sec. S7 A.

Crossovers lines of supercritical water have been investigated in many studies [10, 19, 20, 36, 40, 50, 65–67], using various definitions listed in Table S1. Figure S8(A) shows the phase diagram of water [68], where we have included thermodynamic crossover lines L^\pm . The original EOS data are collected from the NIST database [11], and L^\pm are determined in the same way as for argon (see Fig. S8(B) for an enlarged view).

S5. LINEAR SCALING THEORY

A. Sketch of the theory

Near a critical point, the thermodynamic potential $\Psi(h_1, h_2)$ is a homogeneous function,

$$\Psi(h_1, h_2) = |h_2|^{2-\alpha} f(h_1/|h_2|^{\beta+\gamma}), \quad (\text{S12})$$

of two independent scaling fields h_1 and h_2 [69–72]. Here h_1 and h_2 are the *ordering field* and *thermal field*, $f(x)$ is a universal scaling function, and α , β and γ are universal critical exponents interrelated by the scaling relationship $\alpha + 2\beta + \gamma = 2$. We follow Ref. [17] and express h_1 and h_2 as linear combinations of physical fields P and T ,

$$\begin{aligned} h_1 &= \Delta\hat{P} \cos \varphi - \Delta\hat{T} \sin \varphi, \\ h_2 &= \Delta\hat{P} \sin \varphi + \Delta\hat{T} \cos \varphi. \end{aligned} \quad (\text{S13})$$

Here $\Delta\hat{P} = P/P_c - 1$, $\Delta\hat{T} = T/T_c - 1$, and $\tan \varphi = d\hat{P}/d\hat{T}$ is the slope of the coexistence line. For *symmetric* systems (e.g., the Ising model and the lattice-gas model), $\varphi = 0$: in this case the ordering field $h_1 = \Delta\hat{P}$ and the thermal field $h_2 = \Delta\hat{T}$. Real liquid-gas transitions are generally considered as *asymmetric*, because $\varphi \neq 0$; consequently the physical fields P and T are mixed of h_1 and h_2 .

For practical use, it is convenient to employ a parametric representation of h_1 and h_2 . The linear scaling theory [73, 74] provides the simplest form of parameterization, which expresses h_1 and h_2 with “polar” variables r and θ :

$$\begin{aligned} h_1 &= ar^{\beta\delta}\theta(1 - \theta^2), \\ h_2 &= r(1 - b^2\theta^2), \end{aligned} \quad (\text{S14})$$

where δ is an independent exponent satisfying the scaling relation $(\delta - 1)\beta = \gamma$, a is a system-dependent fitting parameter, and b is a universal parameter obeying $b^2 = (\delta - 3)/(\delta - 1)(1 - 2\beta)$. The variable r represents a “distance” from the critical point, and $\theta \in [-1, 1]$ is a measure of the “angle” from the coexistence line (the coexistence line corresponds to $\theta = \pm 1$). With the parameterization Eq. (S14), Eq. (S12) becomes,

$$\Psi(r, \theta) = r^{\beta(\delta+1)}p(\theta), \quad (\text{S15})$$

where $p(\theta)$ is an analytical function.

The order parameter conjugated to h_1 is

$$\begin{aligned} \phi_1 &= \left(\frac{\partial \Psi}{\partial h_1} \right)_{h_2} = \frac{\partial \Psi}{\partial r} \frac{\partial r}{\partial h_1} + \frac{\partial \Psi}{\partial \theta} \frac{\partial \theta}{\partial h_1} \\ &= r^\beta m(\theta) \\ &= kr^\beta \theta, \end{aligned} \quad (\text{S16})$$

where $m(\theta)$ is related to $p(\theta)$ in Eq. (S15), which is in general unknown. In the last equality, $m(\theta)$ is assumed to be a linear function of θ , $m(\theta) = k\theta$, hence the name linear scaling theory [73, 74]. Here k is another system-dependent fitting parameter. Similarly, the order parameter conjugated to h_2 can be calculated,

$$\begin{aligned} \phi_2 &= \left(\frac{\partial \Psi}{\partial h_2} \right)_{h_1} = \frac{\partial \Psi}{\partial r} \frac{\partial r}{\partial h_2} + \frac{\partial \Psi}{\partial \theta} \frac{\partial \theta}{\partial h_2} \\ &= r^{\beta(\delta+1)-1}s(\theta). \end{aligned} \quad (\text{S17})$$

The function $s(\theta)$ can be determined from the equality $\left(\frac{\partial \phi_1}{\partial h_2} \right)_{h_1} = \left(\frac{\partial \phi_2}{\partial h_1} \right)_{h_2}$, giving,

$$s(\theta) = ak(s_0 + s_2\theta^2), \quad (\text{S18})$$

where,

$$\begin{aligned} s_0 &= -\frac{\beta[-3 + \delta + b^2(-1 + \delta)(-2 + \beta + \beta\delta)]}{2b^4(-2 + \beta + \beta\delta)(-1 + \beta + \beta\delta)}, \\ s_2 &= \frac{\beta(\delta - 3)}{2b^2(-2 + \beta + \beta\delta)}. \end{aligned} \quad (\text{S19})$$

Let us summarize the input to the theory: the critical exponents (β, γ, \dots) determined by the universality class, and three system-dependent parameters including the slope of the coexistence line φ , the parameter a appeared in Eq. (S14), and the parameter k appeared in Eq. (S16). Once these values are given, physical quantities depend only on two independent variables r and θ , and the EOSs are fixed. For example, using Eqs. (S13) and (S14), $\Delta\hat{P}$ and $\Delta\hat{T}$ can be expressed as,

$$\begin{aligned}\Delta\hat{P} &= h_1 \cos \varphi + h_2 \sin \varphi \\ &= ar^{\beta+\gamma}\theta(1-\theta^2) \cos \varphi + r(1-b^2\theta^2) \sin \varphi, \\ \Delta\hat{T} &= h_2 \cos \varphi - h_1 \sin \varphi \\ &= r(1-b^2\theta^2) \cos \varphi - ar^{\beta+\gamma}\theta(1-\theta^2) \sin \varphi.\end{aligned}\tag{S20}$$

The reduced volume is

$$\begin{aligned}\Delta\hat{V} &= \left(\frac{\partial\Psi}{\partial\Delta\hat{P}} \right)_{\hat{T}} = \frac{\partial\Psi}{\partial h_1} \frac{\partial h_1}{\partial\Delta\hat{P}} + \frac{\partial\Psi}{\partial h_2} \frac{\partial h_2}{\partial\Delta\hat{P}} \\ &= -\phi_1 \cos \varphi - \phi_2 \sin \varphi,\end{aligned}\tag{S21}$$

Near the critical point, the reduced density is $\Delta\hat{\rho} = (\rho - \rho_c)/\rho_c \simeq -\Delta\hat{V}$, and therefore

$$\Delta\hat{\rho} = \phi_1 \cos \varphi + \phi_2 \sin \varphi.\tag{S22}$$

Similarly, the reduced entropy is

$$\begin{aligned}\Delta\hat{S} &= - \left(\frac{\partial\Psi}{\partial\Delta\hat{T}} \right)_{\hat{P}} = - \left(\frac{\partial\Psi}{\partial h_1} \frac{\partial h_1}{\partial\Delta\hat{T}} + \frac{\partial\Psi}{\partial h_2} \frac{\partial h_2}{\partial\Delta\hat{T}} \right) \\ &= -\phi_1 \sin \varphi + \phi_2 \cos \varphi.\end{aligned}\tag{S23}$$

The susceptibilities can be computed using the following expressions,

$$\begin{aligned}\chi_1 &\equiv \left(\frac{\partial\phi_1}{\partial h_1} \right)_{h_2} = \frac{k}{a} r^{-\gamma} C_1(\theta), \\ \chi_2 &\equiv \left(\frac{\partial\phi_2}{\partial h_2} \right)_{h_1} = r^{-\alpha} C_2(\theta), \\ \chi_{12} &\equiv \left(\frac{\partial\phi_1}{\partial h_2} \right)_{h_1} = \left(\frac{\partial\phi_2}{\partial h_1} \right)_{h_2} = kr^{\beta-1} C_{12}(\theta),\end{aligned}\tag{S24}$$

where

$$\begin{aligned}C_1(\theta) &= \frac{(1-b^2\theta^2(1-2\beta))}{C_0(\theta)}, \\ C_2(\theta) &= \frac{[(1-\alpha)(1-3\theta^2)s(\theta) - 2s_2\beta\delta\theta^2(1-\theta^2)]}{C_0(\theta)}, \\ C_{12}(\theta) &= \frac{\beta\theta [1-\delta-\theta^2(3-\delta)]}{C_0(\theta)}, \\ C_0(\theta) &= (1-3\theta^2)(1-b^2\theta^2) + 2\beta\delta b^2\theta^2(1-\theta^2).\end{aligned}\tag{S25}$$

Depending on φ , the physical response functions are generally combinations of χ_1 , χ_2 and χ_{12} . For example, the susceptibility (isothermal compressibility) κ_T , the isobaric specific heat C_P , and the isobaric thermal expansion coefficient α_P are,

$$\begin{aligned}\kappa_T &\equiv \left(\frac{\partial\Delta\hat{\rho}}{\partial\Delta\hat{P}} \right)_{\hat{T}} = \left(\frac{\partial\Delta\hat{\rho}}{\partial h_1} \frac{\partial h_1}{\partial\Delta\hat{P}} + \frac{\partial\Delta\hat{\rho}}{\partial h_2} \frac{\partial h_2}{\partial\Delta\hat{P}} \right) = (\chi_1 \cos^2 \varphi + \chi_{12} \sin 2\varphi + \chi_2 \sin^2 \varphi), \\ C_P &\equiv \left(\frac{\partial\Delta\hat{S}}{\partial\Delta\hat{T}} \right)_{\hat{P}} = \left(\frac{\partial\Delta\hat{S}}{\partial h_1} \frac{\partial h_1}{\partial\Delta\hat{T}} + \frac{\partial\Delta\hat{S}}{\partial h_2} \frac{\partial h_2}{\partial\Delta\hat{T}} \right) = (\chi_1 \sin^2 \varphi - \chi_{12} \sin 2\varphi + \chi_2 \cos^2 \varphi), \\ \alpha_P &\equiv \left(\frac{\partial\Delta\hat{V}}{\partial\Delta\hat{T}} \right)_{\hat{P}} = \left(\frac{\partial\Delta\hat{V}}{\partial h_1} \frac{\partial h_1}{\partial\Delta\hat{T}} + \frac{\partial\Delta\hat{V}}{\partial h_2} \frac{\partial h_2}{\partial\Delta\hat{T}} \right) = \frac{1}{2} [(\chi_1 - \chi_2) \sin 2\varphi - 2\chi_{12} \cos 2\varphi].\end{aligned}\tag{S26}$$

Below we show that, independent of φ , the pressure and order parameter $\Delta\hat{\rho}$ on the supercritical crossover lines satisfy the following scalings (identical to Eqs. (3) and (4)),

$$|\delta\hat{P}^\pm| \sim \Delta\hat{T}^{\beta+\gamma}, \quad (\text{S27})$$

where $\delta\hat{P} = \Delta\hat{P}(\Delta\hat{\rho}; \hat{T}) - \Delta\hat{P}(0; \hat{T})$ with $\Delta\hat{P}(0; \hat{T})$ the reduced pressure on the critical isochore, and

$$|\Delta\hat{\rho}^\pm| \sim \Delta\hat{T}^\beta. \quad (\text{S28})$$

Note that on the critical isochore, the reduced density is $\Delta\hat{\rho} = 0$.

B. Symmetric model with $\varphi = 0$

When the slope of the coexistence line is zero, i.e., $\varphi = 0$, the scalings Eqs. (S27) and (S28) can be derived analytically [17]. In this case,

$$\begin{aligned} \Delta\hat{P} &= h_1 = ar^{\beta+\gamma}\theta(1-\theta^2), \\ \Delta\hat{T} &= h_2 = r(1-b^2\theta^2), \\ \Delta\hat{\rho} &= \phi_1 = kr^\beta\theta, \end{aligned} \quad (\text{S29})$$

from which we can get $r = \left[\frac{\Delta\hat{P}}{a\theta(1-\theta^2)}\right]^{1/(\beta+\gamma)}$. The response functions Eqs. (S26) become,

$$\kappa_T = \frac{k}{a}r^{-\gamma}C_1(\theta) = \frac{k}{a}\left[\frac{a\theta(1-\theta^2)}{\Delta\hat{P}}\right]^{\gamma/(\beta+\gamma)}C_1(\theta). \quad (\text{S30})$$

$$C_P = r^{-\alpha}C_2(\theta) = \left[\frac{a\theta(1-\theta^2)}{\Delta\hat{P}}\right]^{\alpha/(\beta+\gamma)}C_2(\theta), \quad (\text{S31})$$

$$\alpha_P = -kr^{\beta-1}C_{12}(\theta) = -k\left[\frac{a\theta(1-\theta^2)}{\Delta\hat{P}}\right]^{(1-\beta)/(\beta+\gamma)}C_{12}(\theta). \quad (\text{S32})$$

For a fixed $\Delta\hat{P}$, a response function reaches its extreme value at a constant θ : $\theta_1 = \pm 0.526$, $\theta_2 = \pm 0.925$ and $\theta_{12} = \pm 0.743$ for κ_T , C_P and α_P respectively. For any response function, because its extreme value is obtained at a constant θ , from Eq. (S29) we can derive universal scalings (S27) and Eqs. (S28), along the line of extremums. Note that, when $\varphi = 0$, $\delta\hat{P} = \Delta\hat{P} - \Delta\hat{P}(\Delta\hat{\rho} = 0; \hat{T}) = \Delta\hat{P}$, since the isochore line is identical to the horizontal axis $\Delta\hat{P}(0; \hat{T}) = 0$.

C. Asymmetric models with $\varphi \neq 0$

When the slope of the coexistence line is not zero, i.e., $\varphi \neq 0$, it is difficult to obtain an analytical expression of L^\pm . One has to compute L^\pm numerically following the procedure described in Sec. S3. Without loss of generality, we use the following setup: the critical exponents are taken from the 3D Ising model universal class, $\beta \simeq 0.3265$ and $\gamma \simeq 1.237$ [45] (other exponents can be computed using the scaling relations $\alpha + 2\beta + \gamma = 2$ and $(\delta - 1)\beta = \gamma$). The slope of the coexistence line is set to be $\varphi = 82^\circ$, which is close to that of many real substrates (such as CO_2 , N_2O , CH_3F , etc.). The parameter a varies from 0.02 to 0.2. To reduce the number of independent parameters, we set $k/a = 1$ following previous studies, as suggested by the Monte Carlo simulations of the 3D Ising model with short range interactions [72, 75]. The numerical solution of crossover lines L^\pm using the linear scaling theory indeed confirms Eqs. (S27) and (S28), as shown in Fig. S9. We emphasize that these universal scalings are independent of the specific choice of parameters.

Interestingly, the scalings Eqs. (S27) and (S28) remain satisfied if one defines the supercritical crossover lines as the lines of extremums of another response function, such as the isobaric specific heat C_P or the isobaric thermal expansion coefficient α_P . Following a similar procedure as described in Sec. S3, such crossover lines can be also

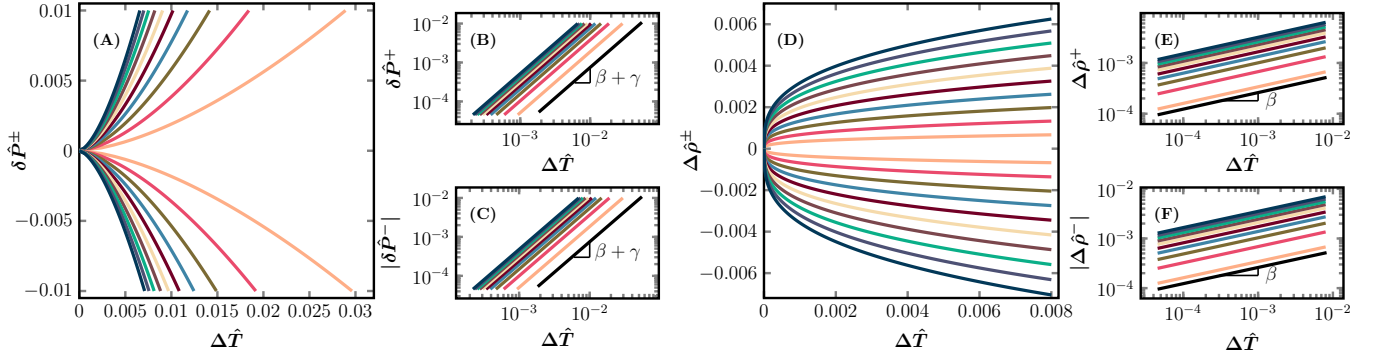


FIG. S9. **Thermodynamic crossover lines L^\pm obtained from the linear scaling theory for asymmetric models** ($\varphi = 82^\circ$). (A) $\delta\hat{P}^\pm$ as a function of $\Delta\hat{T}$ along L^\pm , for $a = 0.02, 0.04, 0.06, 0.08, 0.1, 0.12, 0.14, 0.16, 0.18, 0.2$ (from right to left) and $k = a$. The same data are plotted in log-log scales in (B) and (C) for L^+ and L^- respectively, confirming the scaling Eq. (S27). (D) $\Delta\hat{\rho}$ as a function of $\Delta\hat{T}$ along L^\pm . The same data are plotted in log-log scales in (E) and (F) for L^+ and L^- respectively, confirming the scaling Eq. (S28). The meaning of colors are the same in all panels.

obtained numerically (see Fig. S10). Without loss of generality, we set $\varphi = 82^\circ$ and $a = k = 0.1$. Our results demonstrate that the scalings, Eqs. (S27) and (S28), are independent of which particular response function is used in the definition of L^\pm . While the scalings are universal, Fig. S11 shows that the supercritical crossover lines defined according to different response functions do not completely coincide, in the regime that is not very close to the critical point.

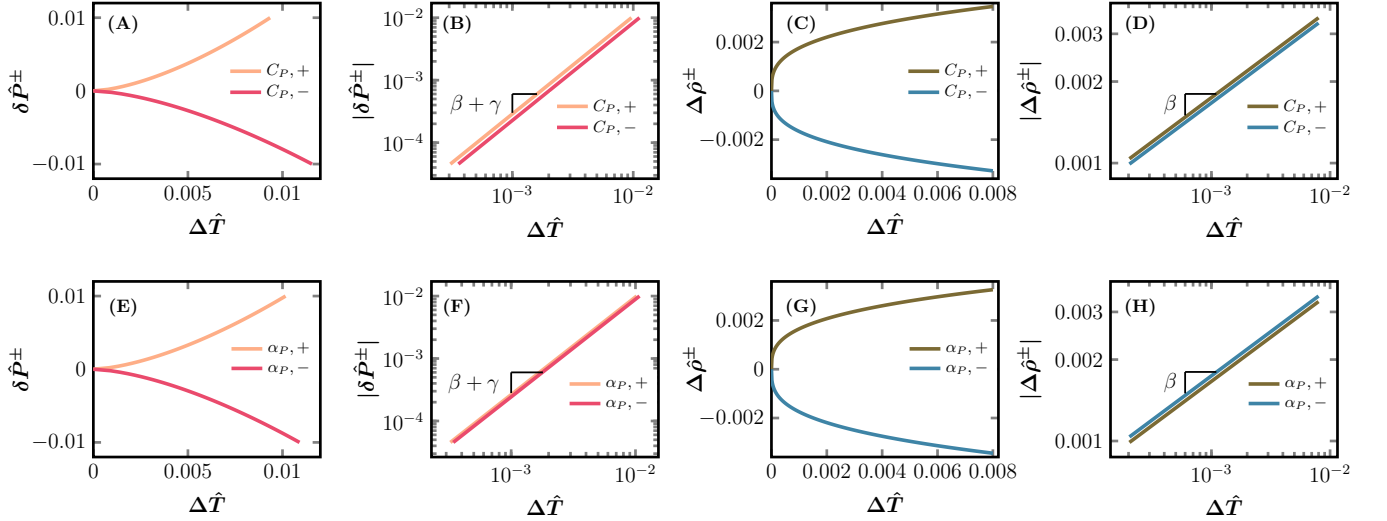


FIG. S10. **Thermodynamic crossover lines L^\pm defined based on other response functions, obtained from the linear scaling theory for an asymmetric model** ($\varphi = 82^\circ$, $a = k = 0.1$). (A) $\delta\hat{P}^\pm$ as a function of $\Delta\hat{T}$ along L^\pm defined according to extreme values of the isobaric specific heat C_P ; (B) same data in log-log scales. (C) $\Delta\hat{\rho}$ as a function of $\Delta\hat{T}$ along L^\pm defined according to C_P ; (D) same data in log-log scales. (E-H) Similar to (A-D), but with L^\pm defined according to extreme values of the isobaric thermal expansion α_P . In all case, the scalings Eqs. (S27) and (S28) are satisfied.

S6. SUMMARY OF THE COEFFICIENTS A_P^\pm AND A_ρ^\pm IN FIG. 3.

Table S2 summarizes the fitting parameters A_P^\pm and A_ρ^\pm for eight different substrates in Fig. 3.

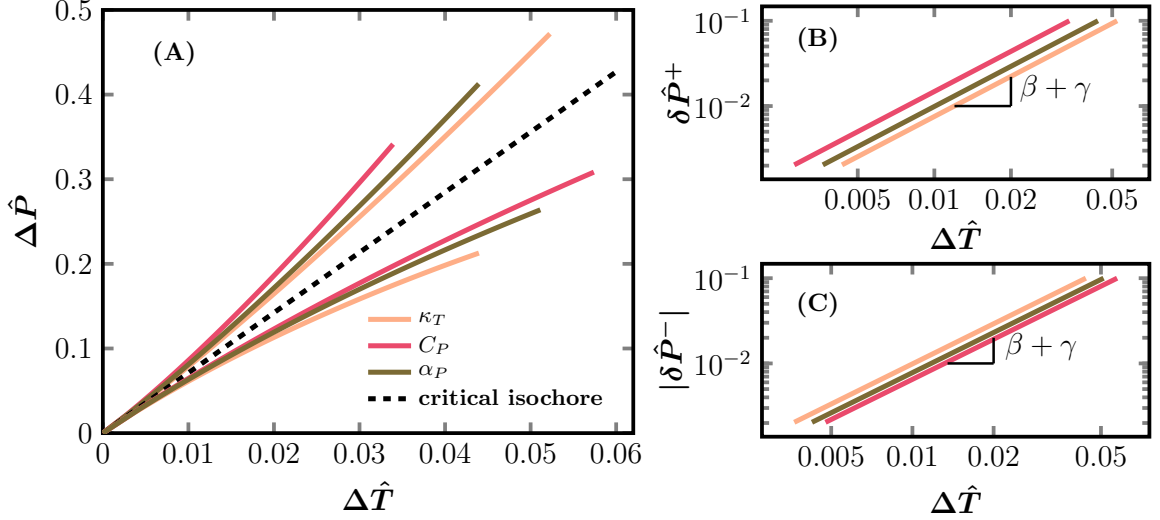


FIG. S11. Comparison of L^\pm defined according to three different thermodynamic response functions in the linear scaling theory. Results are obtained for $\varphi = 82^\circ$ and $a = k = 0.1$. Same data are plotted in log-log scales in (B) and (C).

TABLE S2. Summary of the coefficients A_P^\pm and A_ρ^\pm in Fig.3.

substrates	A_P^+	A_P^-	A_ρ^+	A_ρ^-
Ar	17.31	10.22	0.83	0.97
C ₃ H ₈	21.98	15.08	0.85	0.94
CO ₂	23.39	13.74	0.88	0.99
H ₂ O	23.83	15.54	1.06	0.98
N	18.44	9.97	0.85	0.99
N ₂ O	22.20	13.50	0.85	0.98
Ne	16.58	9.99	0.86	0.99
O ₂	17.99	10.59	0.83	0.98

S7. ADDITIONAL DATA OF L^\pm LINES OF ARGON

A. Examination of different fitting methods

By definition, L^+ is determined at the loci of maxima of κ_T along paths parallel to the isochore. Away from the critical point, the maximum becomes difficult to locate due to the limited range of experimental EOSs. Thus one has to rely on numerical extrapolations to estimate L^+ at pressures much higher than the critical pressure. Based on the scaling obtained from the above theoretical analysis, we fit the data of L^+ near the critical point, which are directly determined from the maxima of κ_T (circles in Fig. 4 and Fig. S12), to,

$$\delta\hat{P}^+ = A_P^+ \Delta\hat{T}^{\beta+\gamma}. \quad (\text{S33})$$

Then the fitting curves are extrapolated to the higher pressure regime (lines in Fig. 4 and Fig. S12), in order to have a full comparison with the sound dispersion data. Two fitting methods are considered. In the first method, we set the 3D Ising model universal class critical exponents $\beta + \gamma = 0.326 + 1.237 = 1.563$, and treat the coefficient A_P^+ as a fitting parameter. In the second method, $\beta + \gamma$ and A_P^+ are treated as two independent fitting parameters. As shown in Fig. S12, the two methods give nearly identical extrapolations in the interested region of the phase diagram.

B. L^\pm lines defined by different response functions

Here we check that if L^\pm lines can be defined using other response functions (see Fig. S13). As shown in Fig. S13A, even though these lines do not completely coincide, the discrepancies reduce approaching the critical point. Further

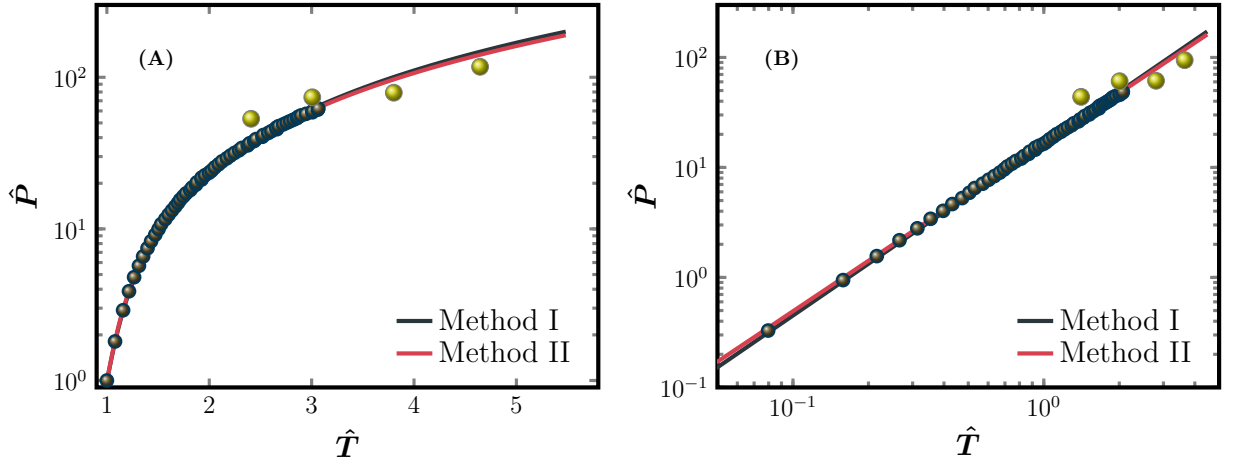


FIG. S12. **Comparison of the extrapolated L^+ line of supercritical argon using two different fitting methods.** (A) Cycles are obtained by locating maxima of κ_T using the NIST data. Solid lines with different colors are obtained using two different fitting methods as described in the text. For the first method (I), the resulted fitting parameter is $A_P^+ = 16.49$. For the second method (II), the resulted fitting parameters are, $A_P^+ = 16.45$ and $\beta + \gamma = 1.523$. Same data are plotted in log-log scales in (B). Yellow balls are dynamical crossovers estimated from the sound dispersion data (see Fig. 4).

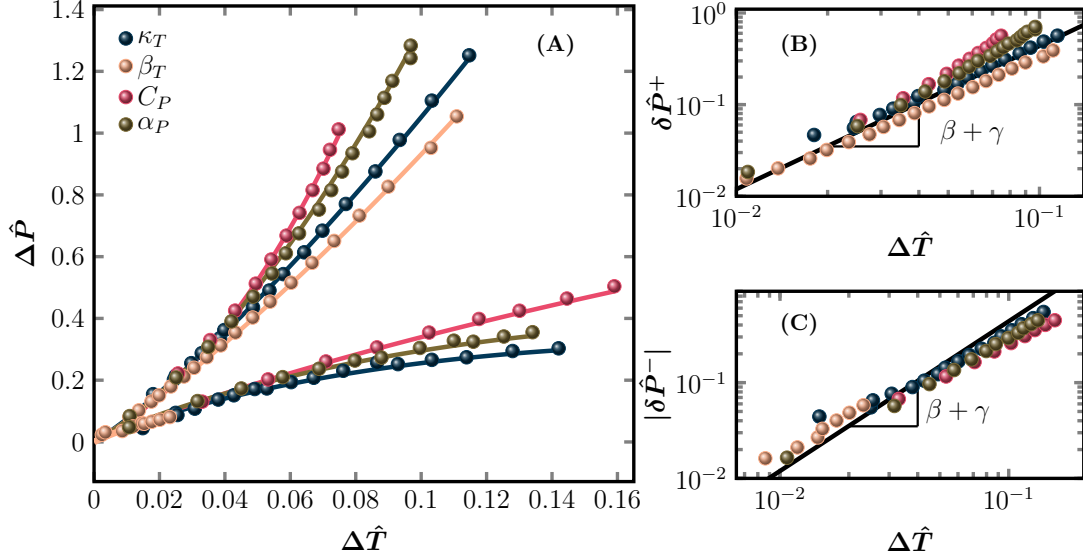


FIG. S13. **Comparison of the L^\pm lines defined according to four different thermodynamic response functions of argon.** (A) L^\pm lines obtained from the maxima of four different response functions, $\kappa_T = \left(\frac{\partial \hat{\rho}}{\partial \hat{P}}\right)_{\hat{T}}$, $\beta_T = \frac{1}{\hat{\rho}} \left(\frac{\partial \hat{\rho}}{\partial \hat{P}}\right)_{\hat{T}}$, $C_P = \hat{T} \left(\frac{\partial \hat{S}}{\partial \hat{T}}\right)_{\hat{P}}$, and $\alpha_P = -\frac{1}{\hat{\rho}} \left(\frac{\partial \hat{\rho}}{\partial \hat{T}}\right)_{\hat{P}}$. (B) and (C) are the same data in log-log scales for L^+ and L^- respectively. Solid lines represent the scaling $\delta \hat{P}^\pm \sim \Delta \hat{T}^{\beta+\gamma}$ with $\beta + \gamma = 1.563$.

more, they follow the same scaling (Fig. S13B and C), consistent with the theoretical results calculated using the linear scaling theory (see Fig. S11). Unlike phase transition lines where all response functions are singular, the thermodynamical crossover lines L^\pm defined by different response functions are not unique, except for the universal scalings. When the crossover line is compared to experimental data, one should choose a proper response function suitable for the given experiment. For example, in the inelastic X-ray scattering experiment, the measured data of sound speed and dispersion are essentially related to density fluctuations [1, 2]; thus it is reasonable to choose κ_T to define L^\pm in order to compare with the data (see Fig. 4 and Sec. S8).

S8. REESTIMATION OF DYNAMICAL CROSSOVERS IN SUPERCRITICAL ARGON FROM SOUND DISPERSION DATA

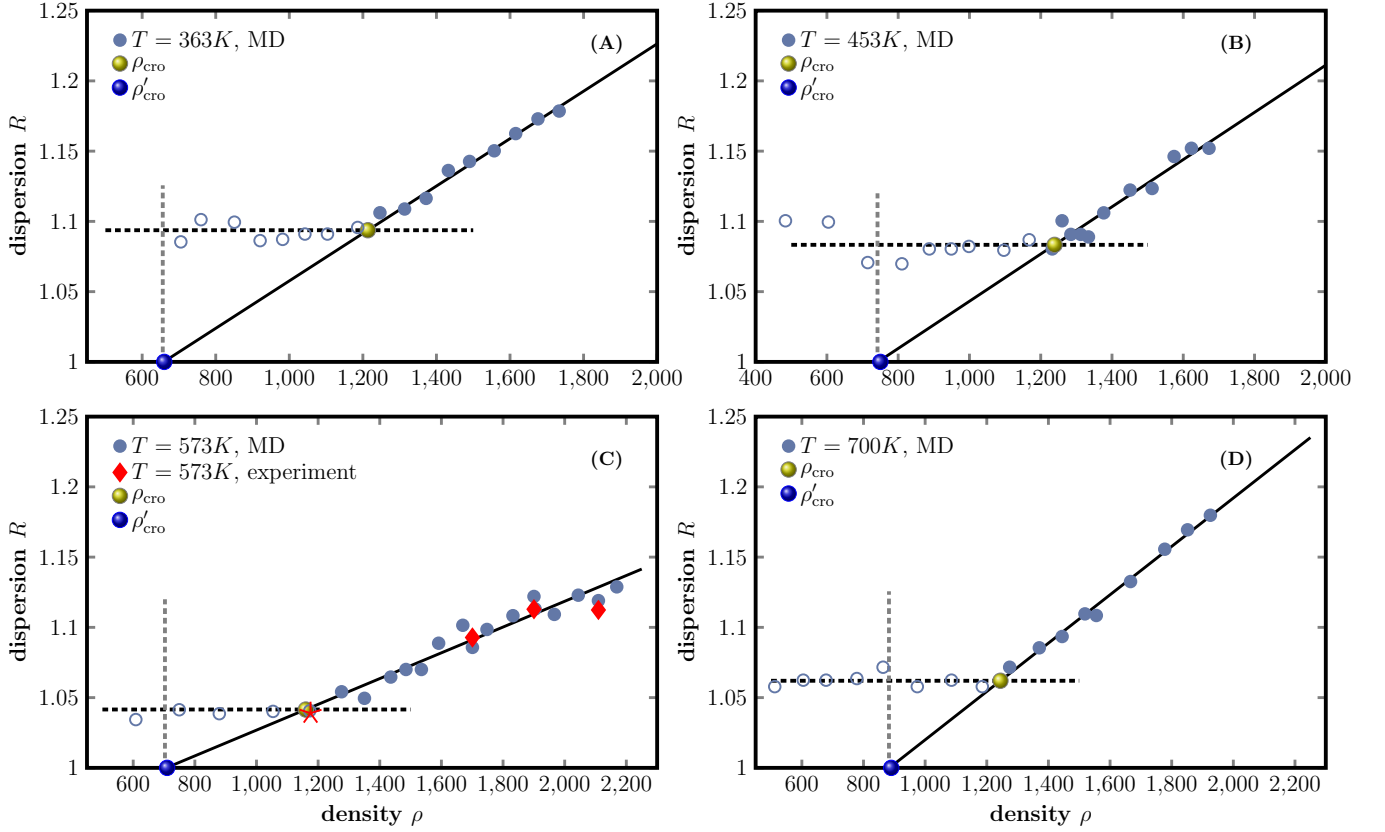


FIG. S14. **Re-estimation of dynamical crossovers in supercritical argon, based on the sound dispersion data collected from [1, 2].** Sound dispersion R as a function of density ρ at four different temperatures. Open and filled circles are data points obtained from molecular dynamics (MD) simulations in [1, 2]. Open circles are fitted to a constant (horizontal dashed line); filled circles are fitted to a linear function (solid line). The intersection of dashed and solid lines defines the crossover density ρ_{cro} . The intersection between the solid line and the $R = 1$ axis defines ρ'_{cro} , according to Ref. [2]. Red diamonds in (C) represent experimental data and the red star represents the crossover estimated in [1].

We collect experimental and simulation sound dispersion data of supercritical argon from the literature [1, 2], and re-analyze them to obtain supercritical crossovers. The data are reported at four temperatures, 363 K ($2.4T_c$), 453 K ($3T_c$), 573 K ($3.8T_c$) and 700 K ($4.6T_c$). Several data points at $T = 573\text{K}$ are obtained from inelastic X-ray scattering experiments in [1] (see Fig. S14); other data points are obtained from molecular dynamics (MD) simulations in [1, 2]. In Fig. S14, we plot the positive dispersion ratio $R = c_L^{\text{max}}/c_s$ as a function of density ρ , where c_L^{max} is the maximum of $c_L(Q)$, $c_s = c_L(Q \rightarrow 0)$ is the adiabatic sound velocity, and $c_L(Q)$ is the longitudinal sound velocity as a function of the wave number Q . A zero value of R means the absence of dispersion.

In Ref. [1], a supercritical dynamical crossover is defined as the separation between a gas-like regime, where $R \approx 1.04$ is a small constant, and a liquid-like regime, where R increases with the pressure P , under a fixed temperature $T = 573\text{K}$. We follow this definition to evaluate the crossover points at other temperatures. Specifically, we fit $R(\rho)$ to a linear function at large ρ , and a constant at small ρ . The intersection of the two lines determines the crossover density ρ_{cro} . Such a method is in fact commonly used in the evaluation of other dynamical crossovers, e.g., the evaluation of liquid-glass transition temperature T_g from heat capacity data. Once $\rho_{\text{cro}}(T)$ is available, $P_{\text{cro}}(T)$ can be computed according to the EOSs provided by the NIST database. Note that our estimated crossover at $T = 573\text{K}$ is fully consistent with the value reported in [1].

In Ref. [2], the authors use another definition to evaluate the supercritical crossovers. The linear fitting of $R(\rho)$ at large ρ is extended to lower ρ ; the intersection between this linear extrapolation and the horizontal line $R = 1$ defines ρ'_{cro} . As can be seen in Fig. S14, ρ'_{cro} obtained in this way is already in the constant $R(\rho)$ regime, and therefore might underestimate the crossover density. Note that the criterion $R = 1$ (i.e., the complete absence of dispersion) is

assumed for the gas or gas-like regime in Ref. [2]. However, according to our phase diagram (Fig. 4), the constant $R(\rho)$ data are in the liquid-gas indistinguishable regime, rather than in the gas-like regime. There is no particular reason to assume that the dispersion is completely absent in the indistinguishable regime: the differences on the acoustic properties of the indistinguishable and gas-like regimes remain to be explored in future studies.

Based on above discussions, we find that ρ_{cro} is a more reliable and accurate estimation of the supercritical crossover density than ρ'_{cro} . Thus the former is adopted in this study.

S9. COMPARISON OF DIFFERENT SUPERCRITICAL CROSSOVER LINES OF ARGON IN THE VICINITY OF THE CRITICAL POINT

In Fig. S15, we compare L^\pm lines with other crossover lines of supercritical argon near the critical point. This is an enlarged view of Fig. 4(A) in the vicinity of the critical point, presented in linear scales.

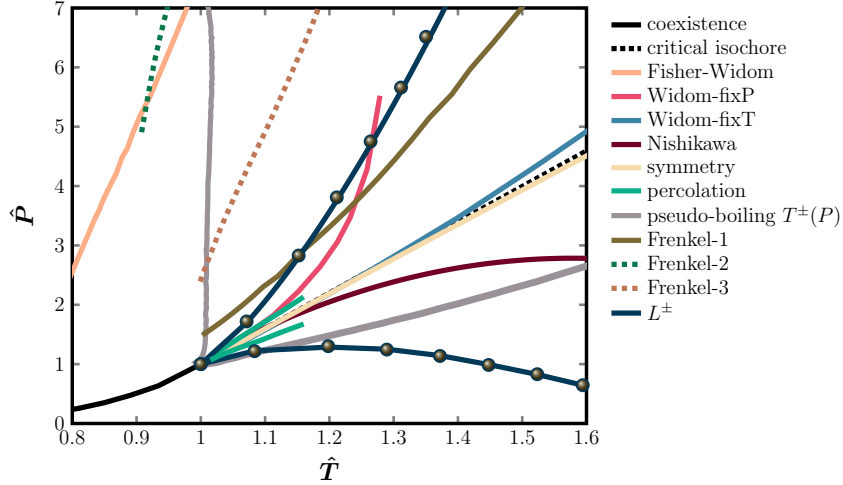


FIG. S15. **Different supercritical crossover lines of argon in the vicinity of the critical point.** This is an enlarged view of Fig. 4(A), and all symbols and colors represent the same meanings as in Fig. 4(A).

S10. NISHIKAWA LINE OF ARGON

Because the Nishikawa line of argon is not available in the literature, here we estimate it according to its definition. The Nishikawa line is determined by the “ridge” of density fluctuations $\frac{\langle(\Delta N)^2\rangle}{\langle N\rangle}$ on the $P - T$ phase diagram. The density fluctuation can be computed from EOSs using the following formula [39]:

$$\frac{\langle(\Delta N)^2\rangle}{\langle N\rangle} = RT\rho\beta_T, \quad (\text{S34})$$

where R is universal gas constant. The data of argon isotherms are collected from the NIST database. Figure S16 shows the colormap and contour lines of density fluctuations on $P - T$ phase diagram, where the Nishikawa line is determined as the ridge of contour lines. The Nishikawa line plotted in Fig. 4(A) is obtained in this way.

S11. VALIDATION OF L^- LINE BY THE EQUATION OF STATES FOR THE COMPRESSIBILITY FACTOR

We show that the L^- line can be validated by the behavior of EOS that relates compressibility factor $Z = PV/nRT$ to $\hat{\rho}$ and \hat{T} , where n is the number of moles. Specifically, the supercritical gas-like states at different \hat{T} obey a single EOS,

$$Z_{\text{gas}}(\hat{\rho}, \hat{T}) - 1 = \mathcal{F} \left[\hat{\rho}/\hat{\rho}^*(\hat{T}) \right], \quad (\text{S35})$$

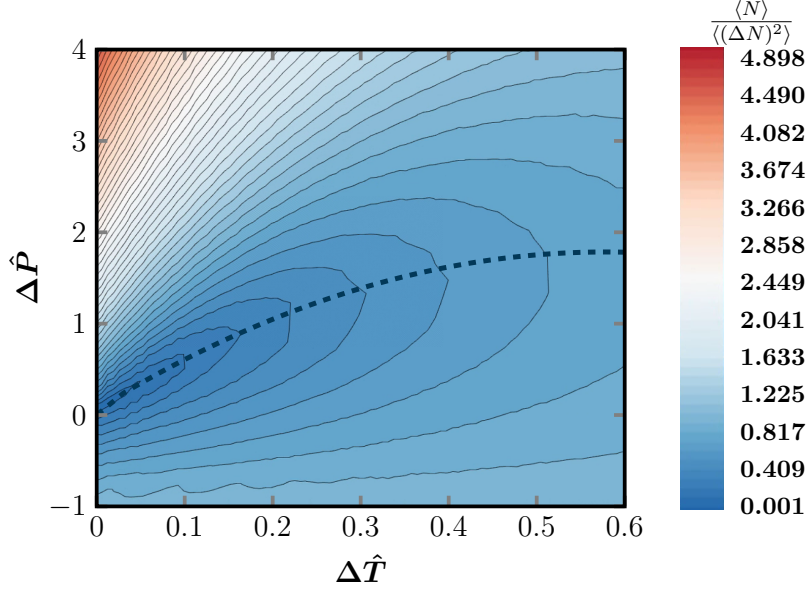


FIG. S16. **Colormap of the density fluctuation** $\frac{\langle(\Delta N)^2\rangle}{\langle N\rangle}$ **in the P - T phase diagram.** Thin solid lines are constant density fluctuation lines. The dashed black line is the ridge that defines the Nishikawa line.

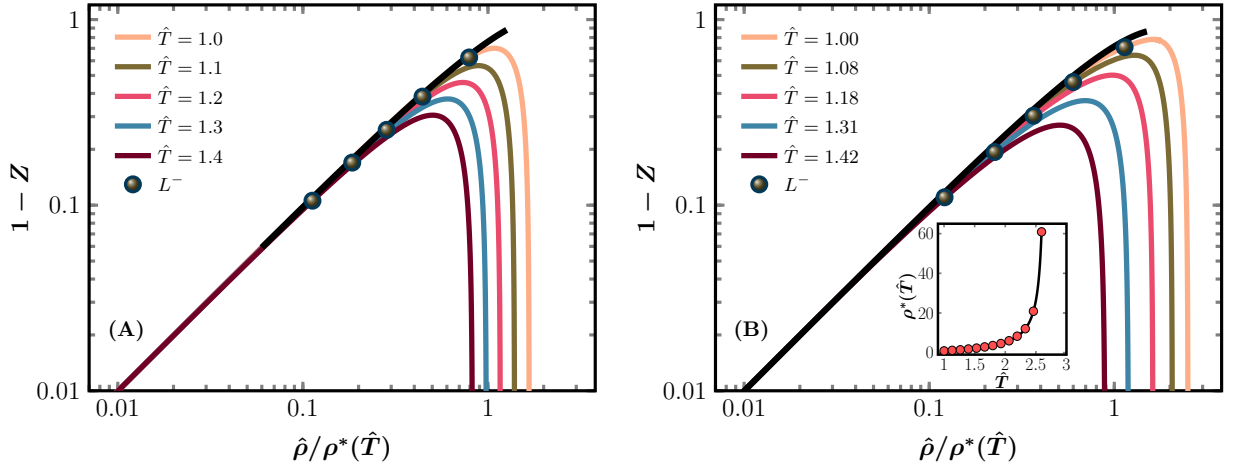


FIG. S17. **Validations of the L^- line by the equation of states for the compressibility factor.** (A) Van der Waals EOS. Colored lines are isotherms and the black line is Eq. (S35) with $\rho^*(\hat{T}) = 24\hat{T}/(27 - 8\hat{T})$ and $\mathcal{F}(x) = -x + 0.24x^2$. (B) NIST data of argon. Colored lines are isotherms and the black line is the fitted gas-like EOS Eq. (S35) with $\mathcal{F}(x) = -x + 0.28x^2$. The points of L^- line are determined independently in Fig. 2, which coincide with the deviation points as shown in the plot. The inset shows $\rho^*(\hat{T})$ as a function of \hat{T} , where the solid line represents $\rho^*(\hat{T}) = 1/(-0.57 + 1.51/\hat{T})$ obtained from fitting.

and that the L^- line coincides with the points where the actual EOS starts to deviate from this gas form. We first derive Eq. (S35) from the van der Waals equation Eq. (S11), which can be rewritten as,

$$Z_{\text{vdW}}(\hat{\rho}, \hat{T}) = \frac{1}{1 - \frac{1}{3}\hat{\rho}} - \frac{9\hat{\rho}}{8\hat{T}}. \quad (\text{S36})$$

In the dilute gas limit $\rho \rightarrow 0$, it can be expanded as,

$$Z_{\text{vdW}}(\hat{\rho}, \hat{T}) \approx 1 + \frac{\hat{\rho}}{3} - \frac{9\hat{\rho}}{8\hat{T}}. \quad (\text{S37})$$

Equation (S37) satisfies the form of Eq. (S35), with $\rho^*(\hat{T}) = 24\hat{T}/(27 - 8\hat{T})$ and $\mathcal{F}(x) \approx -x$. For larger $\hat{\rho}$, Eq. (S35) is still obeyed, with a modified $\mathcal{F}(x) \approx -x + 0.24x^2$ that can be obtained from fitting (see Fig. S17A). The modification

to the dilute-gas EOS with $\mathcal{F}(x) \approx -x$ implies corrections required for high-density gas-like states. At even larger $\hat{\rho}$, Eq. (S35) can no longer be satisfied by modifying $\mathcal{F}(x)$. For a given \hat{T} , the point where the original van der Waals EOS Eq. (S36) deviates from the gas form Eq. (S35) coincides with the L^- line, as shown in Fig. S17(A). This result is consistent with our definition of L^- line: below the line the system is in the gas-like state that can be described by a uniform EOS Eq. (S35); above the line the system enters into the liquid-gas indistinguishable state and thus the gas-like EOS Eq. (S35) does not hold anymore.

We find that the NIST data of argon also follow Eq. (S35) with $\rho^*(\hat{T}) = 1/(-0.57 + 1.51/\hat{T})$ and $\mathcal{F}(x) \approx -x + 0.28x^2$ in the gas-like regime, as shown in Fig. S17(B). For each \hat{T} , the gas-like regime begins from the ideal gas limit ($\rho \rightarrow 0$) and terminates at a point where the EOS deviates from Eq. (S35). The deviation points can be considered as an independent determination of the L^- line, coinciding with those defined in Fig. 2.

S12. COMPARISON BETWEEN DENSITY FLUCTUATIONS ESTIMATED FROM NIST EOSs AND THOSE MEASURED IN SCATTERING EXPERIMENTS

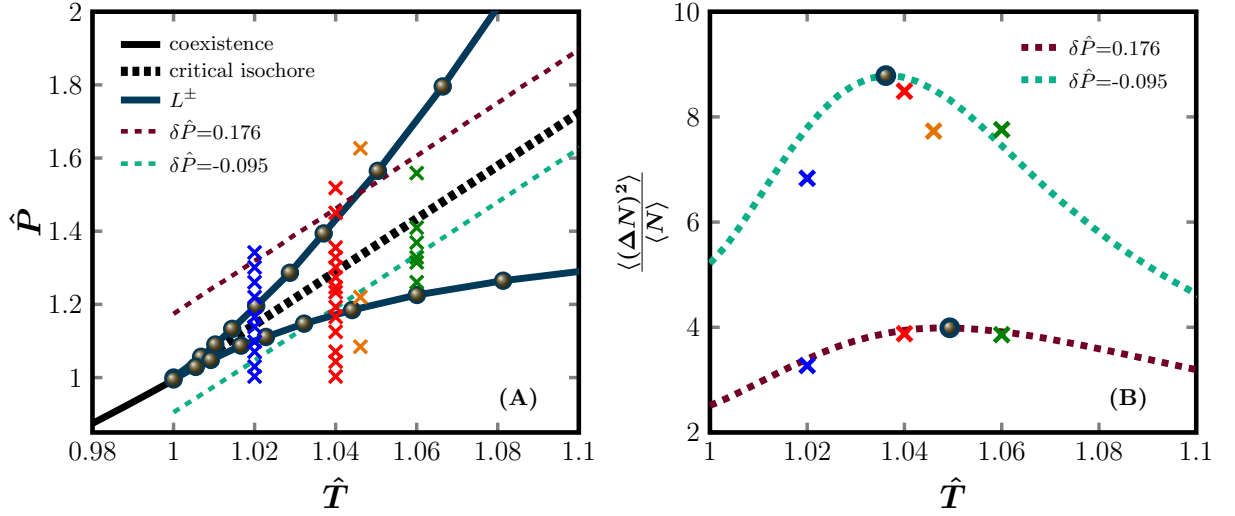


FIG. S18. **Comparison of density fluctuations derived from NIST EOSs with those measured in experiments.** (A) Enlarged $\hat{P} - \hat{T}$ phase diagram Fig. 4B of carbon dioxide CO_2 near the critical point. Experimental data points (crosses) at four different temperatures, $\hat{T} = 1.02$ (blue), $\hat{T} = 1.04$ (red), $\hat{T} = 1.046$ (orange) and $\hat{T} = 1.06$ (green), are collected from Refs. [3, 76]. For the comparison, we choose two example paths parallel to the critical isochore at $\delta\hat{P} = 0.176$ and $\delta\hat{P} = -0.095$. In (B), we plot density fluctuations along the two paths obtained in two different ways. Dashed lines represent density fluctuations obtained using Eq. (S38) based on the NIST EOSs. Crosses represent density fluctuations measured in previous experiments [3, 76]. The L^+ and L^- crossover points (circles) correspond to the maxima of dashed lines.

In the main text (Figs. 2C and D), the susceptibility κ_T is obtained by taking numerical derivatives of the EOSs from the NIST database, and the L^+ and L^- lines are determined by the maxima of κ_T along corresponding paths. The susceptibility κ_T is related to the density fluctuation $\frac{\langle(\Delta N)^2\rangle}{\langle N\rangle}$ by,

$$\frac{\langle(\Delta N)^2\rangle}{\langle N\rangle} = RT\kappa_T. \quad (\text{S38})$$

The density fluctuation can be measured in scattering experiments, but the resolution is limited. To test the reliability of L^+ and L^- lines determined in this study, here we collect the experimental carbon dioxide data from the literature and compare them with the density fluctuations calculated using NIST EOSs. In Fig. S18A, the data points at $\hat{T} = 1.02$, $\hat{T} = 1.04$ and $\hat{T} = 1.06$ were obtained by the small-angle x-ray scattering(SAXS) experiment in Ref. [76], and those at $\hat{T} = 1.046$ were obtained by the small-angle neutron scattering(SANS) experiment [3]. To locate L^+ and L^- crossovers, we take two example paths parallel to the critical isochore, at $\delta\hat{P} = 0.176$ and $\delta\hat{P} = -0.095$. The density fluctuations derived from the NIST EOSs are plotted by dashed lines in Fig. S18B, which are close to the experimental data points. Consequently, the maxima at L^+ and L^- determined from the NIST data are compatible with direct estimates using the experimental data within the resolution.